Experimental Neurology 396 (2026) 115540

Contents lists available at ScienceDirect

Experimental Neurology

journal homepage: www.elsevier.com/locate/yexnr

Research paper

Intranasal delivery of extracellular vesicles derived from human bone marrow mesenchymal stem cells dampens neuroinflammation and ameliorates motor deficits in a mouse model of cortical stroke

Saviana Antonella Barbati [a], Chiara D'Amelio [a], Chiara Feroleto [a,b], Marta Morotti [a,b], Ida Nifo Sarrapochiello [a], Francesca Natale [a,b], Domenica Donatella Li Puma [a,b], Yolanda Gomez-Galvez [c], Elena Blanco-Suarez [c], Lorraine Iacovitti [c], Lucia Leone [a,b], Salvatore Fusco [a,b], Maria Vittoria Podda [a,b,*], Claudio Grassi [a,b]

[a] Department of Neuroscience, Università Cattolica del Sacro Cuore; Rome, Italy
[b] Fondazione Policlinico Universitario A. Gemelli IRCCS; Rome, Italy
[c] Department of Neuroscience, Sidney Kimmel Medical College, Thomas Jefferson University; Philadelphia, PA, USA

ARTICLE INFO

Keywords:
Cytokines
Extracellular vesicles
Functional recovery
Ischemia
Microglia
Motor cortex
Neuroinflammation

ABSTRACT

Early treatment of ischemic stroke can significantly reduce disability and mortality rates. Stem cell-derived extracellular vesicles (EVs) have shown potential as therapeutics for neurological disorders. This study explored whether intranasal administration of EVs from human bone marrow mesenchymal stem cells (BM-MSCs) enhances forelimb motor function recovery in a mouse model of motor cortex stroke and investigated their mechanism of action, focusing on neuroinflammation. C57BL/6JRj mice received EV treatment of 0.1×10^9 EVs per dose per day, 48 h post-stroke and twice weekly for four weeks. EV-treated mice showed significant improvement in forelimb deficits, as evaluated using a series of motor tests. Histopathological assessments revealed reduced infarct volume and decreased astrogliosis and microglial activation in EV-treated mice. EV treatment led to changes in microglial morphology in the peri-infarct area, associated with increased anti-inflammatory cytokines interleukin (IL)-10 and IL-13 and decreased pro-inflammatory cytokines IL-1β, IL-6, and tumor necrosis factor-alpha. Reduced expression of nucleotide-binding oligomerization domain-like receptor protein 3 inflammasome and Cleaved Caspase-1 following EV treatment supports their role in dampening inflammation. In vitro experiments using oxygen-glucose deprivation confirmed that EVs attenuated the inflammatory phenotype of microglia and reduced neuronal apoptosis. EV cargo analysis revealed neuroprotective molecules, including anti-inflammatory cytokines and brain-derived neurotrophic factor (BDNF), which may contribute to their immunomodulatory properties. These findings show that EVs mitigate post-stroke brain immune response, promoting tissue healing and recovery. Our comprehensive characterization of the effects of human BM-MSC-derived EVs, encompassing functional, tissue, cellular, and molecular aspects, underscores their therapeutic potential and supports their use in stroke treatment.

1. Introduction

Stroke is a severe neurological condition resulting from vascular injury, with ischemia accounting for approximately 80 % of cases. Despite the significant burden of this disease, treatment options are limited. However, there is a consensus that early intervention can enhance recovery (Ding and Zhang, 2021). Variability in clinical outcomes, influenced by factors such as the site and extent of the lesion,

Abbreviations: APO-BrdU TUNEL, Apoptosis bromodeoxyuridine terminal deoxynucleotidyl transferase dUTP nick end labeling; BM-MSCs, bone marrow-derived mesenchymal stem cells; hBDNF, human brain-derived neurotrophic factor; DAPI, 4′,6-diamidino-2-phenylindole; EV, extracellular vesicle; GFAP, glial fibrillary acidic protein; GM130, α-Golgi Matrix 130; IL, interleukin; Iba-1, ionized calcium binding adaptor molecule 1; NeuN, neuronal nuclei; NLRP3, nucleotide-binding oligomerization-like receptor protein 3; MCAO, middle cerebral artery; OGD, oxygen-glucose deprivation; ROI, region of interest; TNF, tumor necrosis factor.

* Corresponding author at: Department of Neuroscience, Università Cattolica del Sacro Cuore, Largo F. Vito, 1, 00168 Rome, Italy.
E-mail address: mariavittoria.podda@unicatt.it (M.V. Podda).

https://doi.org/10.1016/j.expneurol.2025.115540
Received 28 July 2025; Received in revised form 16 October 2025; Accepted 29 October 2025
Available online 3 November 2025

poses a significant challenge to treatment efficacy. Most preclinical stroke studies have utilized a rodent model of severe stroke achieved using the filament occlusion model of the middle cerebral artery (MCAO) (Li and Zhang, 2021). While this model replicates many aspects of human stroke, it often results in large ischemic lesions covering nearly the entire hemisphere, leading to severe sensory-motor deficits and high mortality rates. Conversely, experimental models of cortical stroke are increasingly recognized as highly reproducible and robust mild-stroke models with low mortality (Hermann et al., 2019) and precise control of infarct volume, making them ideal for the study of neuroreparative strategies. Despite the smaller infarct area, cortical stroke in patients can have devastating effects on daily activities. For instance, expressive aphasia is observed in frontal lobe strokes, right parietal strokes may lead to neglect syndrome, and motor cortex strokes result in motor impairment, with arm and hand deficits being the most common and debilitating conditions (Murphy and Werring, 2020). Notably, from a translational perspective, given the limited extent of the lesion, therapeutic strategies targeting cortical strokes may have a higher chance of success.

Among recent innovative therapeutic approaches, the systemic administration or transplantation of BM-MSCs has shown great promise. The beneficial effects of these treatments have been documented in animal models of ischemic stroke and in patients (Brenneman et al., 2010; Savitz et al., 2011; Steinberg et al., 2018; Dabrowska et al., 2019; Tsiapalis and O'Driscoll, 2020; Berlet et al., 2021; Davis et al., 2021; Hu et al., 2022). Nonetheless, the development of stroke treatment using EVs derived from BM-MSCs has recently emerged as a novel and potentially safer therapeutic approach, given EVs' low immunogenicity and the absence of risks related to vascular obstruction and tumorigenesis (Tsiapalis and O'Driscoll, 2020). EVs are small microvesicles, 30 to 200 nm in diameter, released by various cell types that contain a variety of cargo molecules, including proteins such as neurotrophins, mRNAs, non-coding RNAs, and lipids. EVs are crucial source of signals for intercellular communication and may account for the beneficial effects of stem cell therapy. Moreover, growing evidence suggests that intranasal delivery is a non-invasive and effective strategy for delivering EVs to the brain for treating neurological disorders (Dhuria et al., 2010; Spinelli et al., 2020; Natale et al., 2022; Zhou et al., 2023).

Considering the aforementioned factors, this study characterized the impact of intranasal administration of human BM-MSC EVs—hereafter referred to as "EVs"—on improving forelimb motor recovery in a photothrombotic mouse model of ischemic stroke targeting the caudal forelimb area of the motor cortex. Our findings revealed that mice treated with EVs showed enhanced performance in motor tests evaluating various aspects of forelimb function and exhibited a reduction in infarct size compared to those treated with the vehicle.

It is well established that, following a stroke, secondary injury mechanisms including inflammation and cell death exacerbate the damage beyond the initial ischemic or haemorrhagic event. This secondary injury involves immune system activation, which triggers inflammation and leads to further neuronal death, even in areas initially spared from direct damage. Consequently, targeting the brain's immune system and dysregulated cytokine expression is considered a promising strategy to modulate brain damage during and after a stroke (Kumari et al., 2024; Moulton et al., 2024). Therefore, this study examined the potential immunomodulatory effects of EVs and demonstrated that they reduced astrogliosis, microglial activation, and the expression of pro-inflammatory cytokines, as well as the nucleotide-binding oligomerization-like receptor protein 3 (NLRP3) inflammasome, the activation of which is a key stage of neuroinflammation and pyroptosis (Xu et al., 2025). Moreover, in vitro experiments using an oxygen-glucose deprivation (OGD) model demonstrated the ability of EVs to mitigate microglial inflammatory response and neuronal apoptosis.

2. Materials and methods

This study adheres to the American Heart Association Journals implementation of the Transparency and Openness Promotion Guidelines. The experiments were designed in accordance with the ARRIVE guidelines (Supplementary Material 1). A complete list of the antibodies used in this study is provided in Supplementary Table 1 (Supplementary Material 2).

2.1. Human BM-MSC culture, EV isolation, characterization, labeling, and administration

Human BM-MSCs were purchased from Celprogen (Headquarters Celprogen Inc., Torrance, CA, USA, #36094–21) and cultured on pre-coated flasks with human BM-MSC culture extracellular matrix for expansion in human (MM-derived) MSC culture complete growth medium without FBS (Headquarters Celprogen Inc., Torrance, CA, USA). Cell supernatants from human MSCs (at passage 2–3) were collected and pre-cleared using a multistep centrifugation protocol. EVs were purified using the exoEasy Maxi Kit (Qiagen, Venlo, Netherlands) according to the manufacturer's instructions. Isolated EVs were subjected to phosphate-buffered saline (PBS) buffer exchange using Vivaspin 2 columns (Sartorius, Goettingen, Germany; cat. Number VS0232) for in vivo treatment (Spinelli et al., 2020).

EVs were analyzed and quantified using a Nanosight NS300 particle size analyzer (NTA; Malvern Panalytical, Malvern, UK). The isolated EVs were resuspended in PBS and stored at −80 °C.

Morphological analysis of EVs was performed by negative stained transmission electron microscopy. Five microliters of isolated EVs were pipetted onto carbon-coated grids (Electron Microscopy Sciences, Hatfield, **PA, USA**, #CF200-CU-50) and incubated for ~5 min. The excess liquid was gently removed, and 2 % uranyl acetate solution was added to the samples. The samples were rinsed with double-distilled water and allowed to dry at room temperature (RT; i.e., 22–24 °C). Sample images were captured using an FEI Tecnai T12 120 kV electron microscope and an AMT XR111 CCD camera.

For the visualization of EVs in vivo, EVs were labeled with the fluorescent membrane dye kit ExoGlow™ (ExoGlow™ Membrane EV Labeling Kit, System Biosciences, Palo Alto, CA, USA, cat. Number EXOGM600A-1), following the manufacturer's instructions. Briefly, Labeling Reaction buffer (composed of 12 μl of Reaction Buffer and 2 μl of Labeling Dye) was mixed with 100 μg of EVs in PBS 1× or PBS 1× alone (negative control). After a 30 min incubation at RT, a single 1 min spin using a buffer exchange column (PD SpinTrap G-25 from Cytiva, Uppsala, Sweden, cat. Number 28918004) was performed to remove the unbound dye. In addition, we performed a reprecipitation protocol with ExoQuick-TC (System Biosciences, Palo Alto, CA, USA) to further clean the sample before proceeding with the downstream applications.

To assess EV localization in brain tissue, mice were treated intranasally with approximately 4 μl PBS (2 μl per nostril) containing 1×10^9 EVs ($n = 3$ mice) or PBS 1× alone (negative control) (n = 3 mice) and 6 h later, the animals were deeply anesthetized, transcardially perfused with PBS (0.1 M, pH 7.4) followed by 4 % paraformaldehyde (PFA) and sacrificed. Brain tissues were collected, post-fixed overnight at 4 °C in PFA, and transferred to a solution of 30 % sucrose in 0.1 M PBS. Coronal brain sections (40-μm-thick) were cut using a vibratome (VT1000S, Leica Microsystems, GmbH, Wetzlar, Germany) and immunoprocessed. After permeabilization and 1 h blocking incubation in PBS 1× with 0.3 % Triton X-100 (Sigma-Aldrich, St. Louis, MO, USA) and 5 % normal goat serum (NGS, Thermo Fisher Scientific, Waltham, MA, USA), tissues were incubated overnight at 4 °C with glial fibrillary acidic protein (GFAP) antibody (1:400). The next day, the tissues were incubated for 90 min at RT with the secondary antibody: Alexa Fluor-488 anti-mouse (1:500). Finally, the nuclei were counterstained with 4′,6-diamidino-2-phenylindole (DAPI, 0.5 μg/ml for 10 min), and the slices were coverslipped with ProLong Gold Antifade reagent (Invitrogen, Waltham, MA,

USA). Images (1024 × 1024 pixels) were acquired at 20× or 40× magnification using a Nikon A1 MP confocal system (Nikon, Tokyo, Japan) and an oil-immersion objective (NA 1.2).

2.2. Mice

Adult male C57BL/6JRj mice of 6–8 weeks old were housed under a 12 h light-dark cycle at ambient temperature of 19–22 °C with water and food available ad libitum.

Male C57BL/6JRj mice were used as the preferred stroke model, given that reduced susceptibility to stroke has been reported in J substrain female mice (Zhao et al., 2019).

A total of 56 mice (28 treated with EVs and 28 treated with vehicle) were used in this study. Efforts were made to limit the number of mice used and to minimize their pain and suffering. All experiments and animal procedures were approved by the Ethics Committee of the Catholic University and were in accordance with the Italian (Ministry of Health guidelines, Legislative Decree No. 116/1992) and European Union (Directive No. 86/609/EEC) legislation on animal procedures (animal protocol #17–39, approved by the Ministry of Health with number 284/2022-PR 2022/05/09).

2.3. Study design

Mice received EV treatment consisting of 0.1×10^9 EVs/dose/day intranasally delivered 48 h after stroke and twice a week for four consecutive weeks thereafter (for a total of nine doses), while vehicle mice received PBS. The dose and treatment regimen were chosen based on previously published studies. In particular, in previous studies (Spinelli et al., 2020; Natale et al., 2022), we intranasally administered our experimental models with a solution containing 3 μg of neural stem cell-derived EVs and repeated the treatment every other day for several weeks. By comparing the Bradford and nanotracking analyses, we verified that the measured absorbance values corresponded to 0.1×10^9 EVs derived from human BM-MSCs.

Mice were randomly allocated to two experimental groups and balanced for age, weight, littermate conditions, and baseline performance in the motor tests. Randomization was performed by assigning random numbers. Motor function was assessed at baseline (24 h before stroke), 48 h post-stroke, before EVs/PBS to determine post-stroke deficits, and then once per week for the entire period of treatment to track the time-course of recovery, as summarized in Fig. 1.

Different tests were used for a comprehensive evaluation of the efficacy of EVs on various aspects of motor function, including forelimb asymmetry, coordination, precise paw placement, force and skilled forepaw abilities.

At the end of the follow-up period (i.e., day 31 after stroke), the mice were sacrificed, and their brains were processed for histological and immunofluorescence analyses. Dedicated groups of EV- and vehicle-treated mice were sacrificed 72 h after stroke for ELISA and Western blotting analyses or 1 week after stroke for immunofluorescence analyses.

An in vitro model of ischemia obtained by OGD was used to test the effects of EVs on microglial inflammatory response and neuronal apoptosis following ischemic insult.

2.4. Photothrombotic stroke

Focal cortical lesions in the motor cortex were induced by Rose Bengal photothrombosis (Longo et al., 2022). Ischemia was induced in the motor cortex area contralateral to the preferred paw, as defined by the cylinder test. Mice were anesthetized with a cocktail of ketamine (87.5 mg/kg) and xylazine (12.5 mg/kg) and placed in a stereotaxic apparatus. The skull was exposed, and the photosensitive dye Rose Bengal (Sigma-Aldrich, St. Louis, MO, USA, cat. Number 330000) was intraperitoneally injected at a dose of 75 μg/g body weight. Five minutes after the dye injection, the skull was illuminated for 15 min. A fiber-optic bundle connected to a cold light source was positioned in the area corresponding to the caudal forelimb motor cortex (1.75 mm lateral to the midline and 0.5 mm anterior to bregma). To avoid activation of the dye elsewhere, only a circular area (3 mm^2) over the motor cortex was left exposed, whereas the rest of the skull was covered with a custom

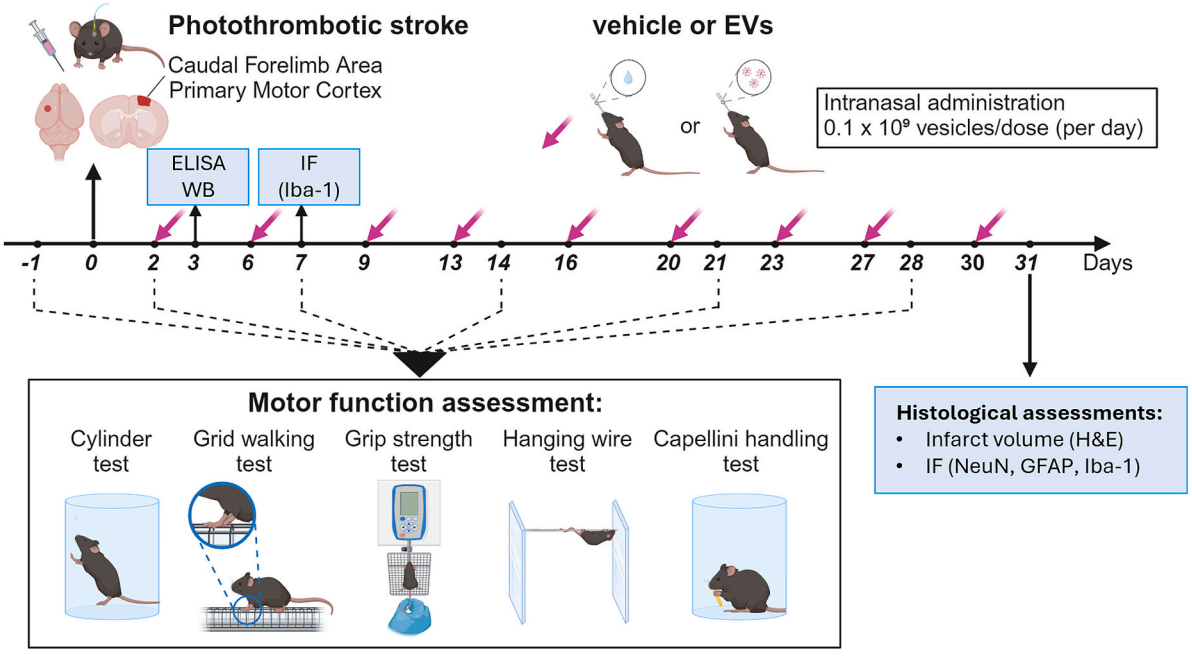

Fig. 1. Experimental timeline. Photothrombotic stroke was induced on day 0. Motor functions were assessed the day before stroke (day −1, baseline), 2 days after stroke, to evaluate post-stroke deficits, and once a week for 4 weeks after stroke in mice treated with vehicle or EVs at the time point indicated by the purple arrows. Infarct volume was determined at the end of treatment by hematoxylin-eosin (H&E) staining together with immunofluorescence analysis (IF) for NeuN, GFAP, and Iba-1. Microglial density and morphology were assessed 1 week post-stroke. ELISA and Western blotting (WB) analyses were performed on day 3 after stroke. Figure was created using Biorender. (For interpretation of the references to colour in this figure legend, the reader is referred to the web version of this article.)

mask.

2.5. Inclusion and exclusion criteria

Animals that did not exhibit significant impairments 48 h after stroke were excluded from the analyses. Significant impairments were defined as follows: <10 % baseline performance in the cylinder test, >3 % foot-faults in the grid-walking test, <20 % baseline performance in the grip strength test, <15 % baseline performance in the hanging wire test, and > 15 % atypical behaviors in the Capellini test. No animal was excluded due to premature death caused by technical complications, and overall, out of 26 mice used for behavioral testing, 6 were excluded only from the analysis of the Capellini test.

2.6. Behavioral tests

2.6.1. Cylinder test

The cylinder test is a spontaneous forelimb use asymmetry test that is relatively straightforward and allows the evaluation of limb preference and post-stroke limb impairment in mice (Schallert et al., 2000; Bakreen et al., 2021). Briefly, the mice were placed inside a plexiglass cylinder, 10 cm in diameter and 15 cm in height. The cylinder was positioned over a plexiglass support, and a camera under the apparatus recorded the forelimb contacts during the vertical exploration. The scoring criteria for forelimb placement were as follows: (1) The first limb to touch the wall of the cylinder during a full rear was considered a forelimb placement on the wall. If both paws were placed simultaneously on the wall during the full rear, the placement was scored as both paw placements. (2) The first limb touching the floor at the end of a single rear-limb movement was considered as a forelimb placement on the floor. If both paws were placed simultaneously on the floor at the end of the rear, placement was scored as both paw placements. The test concluded after a total of 20 vertical movements (20 touches on the wall and 20 touches on the floor) or after a maximum test time of 5 min. The recorded videos were post-processed by a blinded observer during slow motion. The score was calculated as follows: ((impaired forepaw contact +1/2 both contacts)/(non-impaired forepaw contact + impaired forepaw contact + both contacts)) × 100.

2.6.2. Grid walking test

The grid walking test is widely used to measure post-stroke motor coordination deficits. The apparatus consisted of an 11 mm square wire mesh overhead grid (320 × 200 × 500 mm) held by four poles. A camera (Panasonic full HD HC-W580, Osaka, Japan) was used to record 5 min video footage for each mouse while they were allowed to move freely on the grid of the apparatus. A mirror placed 45° under the grid allowed the experimenter to simultaneously visualize at the same time the total step number and stepping errors (i.e., foot faults). A foot fault was considered when a step did not provide support and the paw slipped through a grid hole. Through blinded offline analysis, foot faults along with the total step number performed by each forelimb were counted, and the foot fault percentage was calculated as the number of foot faults/(number of foot faults + number of non-foot-fault steps) × 100 (Longo et al., 2022).

2.6.3. Grip strength test

The grip strength test was used to evaluate motor deficits and functional recovery in stroke mice. Mice were placed in the test room for approximately 30 min prior to the start of the experiment to allow them to familiarize themselves with the surrounding environment. A grip strength meter (Bioseb Instrument, Vitrolles, France) was used to assess the forelimb strength. Mice were allowed to grasp the wire grid of the apparatus with their forepaws while the animal was gently pulled backward, and the maximum grip strength was recorded. Values are reported as the average of three consecutive attempts normalized to mouse body weight and were used for statistical analysis (Longo et al., 2022).

2.6.4. Hanging wire test

The hanging wire test detects muscle strength and neuromuscular impairment in mice. The test requires the animal to be suspended on an elevated metal wire (1 mm thick) positioned 40 cm from the ground, connecting the two sides of a cage. At the beginning of each test, the animal was placed at the center of the wire, hanging only by its forepaws, and a camera positioned in front of the apparatus was turned on to record the movements of the mice. Their performance was evaluated based on a “reaching” score. At the beginning of each session, the “reaching” score was set to zero. Over the duration of 180 s, the “reaching” score was increased by 1 point every time the mouse reached one side of the wire, the timer was paused, and the mouse was placed at the center of the wire (Boutros et al., 2021).

2.6.5. Capellini test

The Capellini test is a simple quantitative measure of forelimb-skilled motor function and stroke-related impairments (Tennant et al., 2010; Whishaw et al., 2017). The apparatus used for the test consisted of a plexiglass cylinder (diameter: 10 cm; height: 15 cm) with a plexiglass floor. Mice were videotaped while handling a short length of uncooked capellini pasta, with a camera positioned under the plexiglass floor to optimize paw movement. To avoid neophobic responses and ensure that the mice developed their forelimb skills, they were exposed to a few pasta pieces ($n = 3$) in their home cage for four consecutive days before the actual test. The day before the test, animals were deprived of food. During the test sessions, mice were recorded while eating a piece of pasta, with one piece eaten per trial for a total of three consecutive trials. Prior to recording, a piece of pasta was placed inside the chamber to initiate eating and to position the animal appropriately for the camera. The camera was then zoomed 5× to capture the detailed movements of the knuckles on both forepaws. Slow-motion video playback was used to identify the different forelimb and paw postures. Specifically, we categorized these behaviors into three groups: typical, atypical, and other. Typical behaviors include movements that mice normally use to manipulate pasta to guide it inside their mouth, including “grasp” (the paw is placed lower on the pasta) and “guide” (the paw is near the mouth). Atypical patterns are a series of paw positions, including (a) placing the paws together in a symmetrical hold, (b) one paw holding the pasta, and (c) eating from the middle of a piece of pasta. Other postures include those in which mice move their paws into more symmetrical positions, side-by-side, or with interposed digits, normally present only when the pasta piece is very short. Eating time was calculated by summing the time spent eating the pasta piece during each trial and averaging them. We calculated the time spent handling pasta using atypical behaviors and expressed the results as the percentage of time spent using atypical behaviors compared to the total eating time.

2.7. Molecular and morphological analyses

2.7.1. Western blotting

EVs were lysed in PBS containing 1 % sodium dodecyl sulfate (SDS) and 1× protease inhibitor cocktail. Lysates were then sonicated for 5 min using a Bioruptor Standard Waterbath Sonicator (Diagenode, Liège, Belgium) and centrifuged for 10 min at 13000 rcf, at 4 °C. All samples were resolved by SDS-polyacrylamide gel electrophoresis under reducing conditions. Proteins were blotted onto a nitrocellulose membrane (Amersham Protran, Cytiva, Uppsala, Sweden, cat. Number 10600015) and probed with the following antibodies: α-HSP70 (1:1000), α-Golgi Matrix (GM)130 (1:1000), α-Alix (3A9) (1:1000), α-CD9 (1:1000), and α-CD81 (EPR 4244) (1:1000). All experiments were independently repeated three times. Protein expression was evaluated using the UVItec Cambridge Alliance (UVItec, Cambridge, UK). Molecular weights were determined using Precision Plus Protein Dual Colour Standards (Bio-Rad, Hercules, CA, USA).

Total proteins were extracted from the perilesional cortex of stroke mice sacrificed 72 h after stroke using ice-cold RIPA buffer, as previously

reported (Longo et al., 2022). Protein lysates (30 μg) were loaded onto 12 % Tris-glycine polyacrylamide gel for electrophoretic separation. Precision Plus Protein™ Dual Colour Standards (Bio-Rad, Hercules, CA, USA) were used as molecular mass standards. The following primary antibodies were used: anti-rabbit Caspase-1 (1:1000), anti-rabbit Cleaved Caspase-1 (Asp296) (1:1000) anti-rabbit anti-NLRP3 (1:1000) (Coll et al., 2015). After three 10-min washes in Tris-buffered saline, 0.1 % Tween 20 (TBST), membranes were incubated for 1 h at RT with horseradish peroxidase (HRP)-conjugated secondary antibodies (1:2000). The membranes were washed again with TBST, and the bands were visualized using an enhanced chemiluminescence detection kit (GE Healthcare, Buckinghamshire, UK). Protein expression was evaluated and documented using UVItec Cambridge Alliance (UVItec, Cambridge, UK). As ischemic conditions may affect the expression of common housekeeping proteins such as glyceraldehyde-3-phosphate dehydrogenase (GAPDH), we adopted total protein normalization via Ponceau S staining for more reliable quantification. Following electrophoretic transfer onto nitrocellulose membranes, blots were incubated for 1–5 min in 0.1 % Ponceau S in 1 % acetic acid diluted 1:3 in TBST and then rinsed with water until the background was clear and digitally scanned. The signal intensities of the target protein bands were quantified and divided by the total protein signal of the respective lane. The stain was removed before standard immunodetection and data analysis.

2.7.2. Hematoxylin-eosin staining

Histological evaluation was performed to calculate the lesion volume. At the end of the treatment and testing periods, the animals were anesthetized using an intraperitoneal injection of a combination of ketamine (87.5 mg/kg) and xylazine (12.5 mg/kg). The mice were then transcardially perfused with saline, followed by a fixative solution containing 4 % PFA in 0.1 M PBS. The brains were subsequently removed from the skulls, post-fixed overnight in 4 % PFA, and stored at 4 °C in a high sucrose solution (30 % sucrose in 0.1 M PBS) for two days. Serial coronal sections (40 μm thick) containing the motor cortex region were cut using a vibratome (Leica VT1000S, Leica Biosystems, Wetzlar, Germany). To assess the infarct size, eight sections spaced 240 μm apart were stained using a hematoxylin-eosin staining kit in accordance with the manufacturer's instructions (Abcam, Cambridge, UK, cat. Number ab245880). Images of the sections were captured using an Axiophot microscope (Zeiss, Oberkochen, Germany) with a 5× objective lens. Subsequently, to obtain images of the entire section, each 5× image of one slice was stitched using the Image Composite Editor program. The ischemic region was identified and quantified using the ImageJ software. The lesion volume for each animal was calculated by summing all damaged areas and multiplying the number by the section thickness (40 μm) and by 6 (spacing factor) (Lai et al., 2015).

2.7.3. Immunofluorescence assays

Sections were rinsed in PBS, blocked at RT for 1 h in a solution containing 1 % bovine serum albumin (BSA, Sigma-Aldrich, St. Louis, MO, USA), 10 % NGS (Thermo Fisher Scientific, Waltham, MA, USA), and 0.5 % Triton X-100 (Sigma-Aldrich, St. Louis, MO, USA), and incubated overnight with the following primary antibodies: Neuronal Nuclei (NeuN, 1:100), GFAP (1:100), and ionized calcium-binding adaptor molecule 1 (Iba1–1, 1:100) at 4 °C. The following day, the sections were thoroughly washed and incubated with the following secondary antibodies: AlexaFluor-488 (1:500) and AlexaFluor-546 (1:500). Cell nuclei were counterstained with DAPI (0.5 μg/ml). The sections were mounted on glass slides and covered with the ProLong Gold Antifade Reagent (Invitrogen, Waltham, MA, USA).

The number of labeled cells in the perilesional region was analyzed using confocal microscopy. The peri-infarct region was defined as a region extending 300 μm beyond the border of the infarct region (Cai et al., 2019). For each animal used for the immunofluorescence assays, two sections (40 μm-thick) representative of both the anterior part of the lesion (between +1.54 and + 1.78 mm from the bregma) and the posterior portion of the lesion (between +0.5 and + 0.74 mm from the bregma) were used. Images (1024 × 1024 pixels) of each marker were acquired at 20× magnification by using a Nikon A1 MP confocal system (Nikon, Tokyo, Japan). High-magnification images (60×) of GFAP and Iba-1 immunostaining were also acquired using an oil-immersion objective (NA 1.2). Immunofluorescence was quantified in three regions of interest (ROIs; 70 × 70 μm) in the peri-infarct area. The ROIs were positioned 100, 200, and 300 μm beyond the scar border. $DAPI^+$ double-labeled cells with NeuN, GFAP, or Iba-1 were counted inside each of the three ROIs. Data obtained from the analysis of the two sections per animal were averaged and expressed as the mean number of double labeled cells/ROIs ± SEM. Two 40 μm-thick slices per animal were used to analyze the area and width of the glial scar. Images (1024 × 1024 pixels) of GFAP were acquired at 20× magnification using a Nikon A1 MP confocal system (Nikon, Tokyo, Japan). The glial scar area was determined by drawing a line around the glial scar (defined as the region in which 100 % of the cells were $GFAP^+$) using a freehand selection tool (NIS-Elements Confocal Software, Tokio, Japan). Glial scar width was defined as the distance between the edges of the glial scar at the widest point.

2.7.4. Microglia morphological analysis

Two 40 μm-thick slices per animal were immunolabeled with Iba-1 (Iba1/AIF-1) (1:100) to visualize microglial cells. For morphological analysis of microglial cells, images (1024 × 1024 pixels) were acquired in the primary motor cortex within the peri-infarct area using a Nikon A1 MP confocal system (Nikon, Tokyo, Japan) with a 60× oil immersion objective (NA 1.2) and a z step of 2 μm. Maximal intensity projections of each image were generated, binarized, and skeletonized using the Skeletonize 2D/3D plugin in ImageJ, after which the Analyze Skeleton plugin (https://imagej.net/AnalyzeSkeleton) was applied. Only the cells whose cell bodies and processes were fully contained in the slices were included in the analysis. The soma area was determined by drawing a line around the cell body using the freehand selection tool. The extent of microglial ramification was quantified by measuring the area circumscribed by the distal ends of each process using the polygon selection tool (arborization area) (Tremblay et al., 2012; Morrison and Filosa, 2013). The number of branches per cell was recorded for each image with a voxel size exclusion limit of 150. The morphological index was calculated as the soma/arborization area.

2.7.5. Enzyme-Linked Immunosorbent Assay (ELISA)

The peri-infarct cortical area from both vehicle- and EV-treated mice was disrupted with a homogenizer and analyzed for the protein content of the following cytokines: IL-10, IL-1β, IL-13, IL-6, and tumor necrosis factor (TNF)-α using a sandwich ELISA, following the manufacturer's instructions (ELISA Flex: Mouse IL-10 [HRP], Mabtech AB, Nacka Strand, Sweden, cat. Number #3432-1H), (ELISA Flex: Mouse IL-1β/IL-1F2, R&D Systems, Minneapolis, MN, USA, cat. Number #DY401) (ELISA Flex: Mouse IL-13 ELISA Kit, R&D Systems, Minneapolis, MN, USA, cat. Number #CSB-E04602) (ELISA Flex: Mouse IL-6 [HRP], Mabtech AB, Nacka Strand, Sweden, cat. Number #3361–1H) (ELISA Flex: Mouse TNFα [HRP], Mabtech AB, Nacka Strand, Sweden, cat. Number #3511–1H). Briefly, 96-well ELISA microplates were coated overnight with monoclonal antibodies against IL-10, IL-1β, IL-13, IL-6, and TNF-α. Samples and standards for each cytokine were added at the appropriate dilution (10 μl of sample in 90 μl of dilution buffer), and the total protein content was quantified using a bicinchoninic acid (BCA) assay (Micro BCA Protein Assay Kit CAT#SH254071, Thermo Fisher Scientific, Waltham, MA, USA). Samples and standards were incubated for 2 h at RT. After careful washing, the respective biotinylated forms (biotinylated-mAb IL-10, biotinylated-mAb IL-1β, biotinylated-mAb IL-13, biotinylated-mAb IL-6 and biotinylated-mAb TNF-α) were added to each well; Streptavidin-horseradish peroxidase was used as the secondary antibody. Absorbance at 450 nm was measured using a VICTOR X4 (Perkin Elmer, Waltham, MA, USA).

The total amounts of IL-1β, IL-10, IL-13, IL-6, and TNF-α proteins analyzed in the samples were normalized to the initial protein content (in mg) of each sample and expressed as pg/mg of protein.

Analysis of EV cargo was performed using ELISA. For each EV preparation, 15×10^9 human BM-MSC EVs were lysed in PBS 1× with protease inhibitors. The samples were sonicated on ice with five 30-s pulses and a 30-s interpulse interval. Sample debris was removed by centrifugation. Three different EV preparations were analyzed in triplicate (2.5×10^9 EVs per well). Human BDNF (hBDNF) content was evaluated using a commercial hBDNF ELISA kit (IK10144, Immunological Sciences, Rome, Italy). The assay was performed following the manufacturer's instructions. Briefly, 100 μl of EV samples (diluted 1:2) were loaded into pre-coated wells and incubated for 90 min at 37 °C. After washing, biotin-labeled anti-BDNF antibody and HRP-streptavidin conjugate were added sequentially, followed by incubation and wash steps. 3,3′,5,5′-tetramethylbenzidine (TMB) substrate was then added, and the reaction was stopped using an acid solution. Absorbance was measured at 450 nm using a microplate reader, and BDNF concentration was interpolated from the standard curve (range: 31.25–2000 pg/ml). The assay was sensitive to 18.75 pg/ml and specific to hBDNF, with no detectable cross-reactivity.

Human cytokines were analyzed by Q-Plex™ Human Cytokine Screen (16-Plex) (#110933HU, Quansys Biosciences, Logan, UT, USA) according to the manufacturer's instructions. 50 μl of each sample (diluted 1:2) was added to each well. The multiplex ELISA kit contains in each well antibodies for detection of the following targets: IL-1α (Lower Limit of Quantification – LLOQ: 4.3 pg/ml), IL-1β (LLOQ: 12.49 pg/ml), IL-2 (LLOQ: 5.66 pg/ml), IL-4 (2.39 pg/ml), IL-5 (3.92 pg/ml), IL-6 (3.41 pg/ml), IL-8 (2.28 pg/ml), IL-10 (9.94 pg/ml), IL-12p70 (3.54 pg/ml), IL-13 (3.72 pg/ml), IL-15 (12.39 pg/ml), IL-17A (21.57 pg/ml), IL-23 (50.58 pg/ml), IFNγ (9.43 pg/ml), TNF-α (6.75 pg/ml), TNFβ (4.86 pg/ml). Each EV sample was analyzed in triplicate. A total of 2.5×10^9 EVs were loaded into each well.

2.8. In vitro OGD experiments on microglial and neuronal cell cultures

Mixed glial cultures were established from postnatal (P0-P2) C57BL/6 mouse pups of either sex according to previously published protocols (Mizrachi and Diamond, 2024) with some modifications. Briefly, after dissection, the brain cortices were incubated for 15 min at 37 °C with 0.25 % trypsin (Thermo Fisher Scientific, Waltham. MA, USA) and gently dissociated by trituration using a fire-polished Pasteur pipette. The cells were plated on poly-L-lysine (Merck, Darmstadt, Germany)-coated flasks in complete DMEM containing 4.5 g/l glucose, supplemented with 10 % fetal bovine serum (FBS, Thermo Fisher Scientific, Waltham. MA, USA), 1 % penicillin-streptomycin (Thermo Fisher Scientific, Waltham. MA, USA), and 0.5 ng/ml of recombinant mouse GM-CSF (Merck, Darmstadt, Germany).

After 14 days of growth to a mixed confluent astrocyte/microglia population, the microglia were isolated using the mild-trypsin method (Saura et al., 2003) and plated at a density of 170.000 cells on 20-mm coverslips (for immunofluorescence analysis) pre-coated with poly DL-ornithine hydrobromide (50 μg/ml; Merck, Darmstadt, Germany). The microglia cultures used were ~ 80 % pure, as assessed by Iba-1 immunoreactivity.

Once the cells reached ~80 % confluency, they were subjected to OGD as an in vitro model of ischemia. Briefly, the cell cultures were exposed to a hypoxic environment with 1 % O_2, 5 % CO_2, and 94 % N_2 for 3 h in a hypoxia chamber (Stemcell Technologies, Vancouver, BC, Canada 27,310) placed in a humidified incubator at 37 °C. Before placing the cultures in the hypoxia chamber, the culture medium was replaced with glucose-free DMEM (Gibco Dulbecco's Modified Eagle Medium cat. Number 31053–028, Thermo Fisher Scientific, Waltham, MA, USA) pre-equilibrated in a hypoxic environment. After 3 h, the cells were removed from the hypoxia chamber, and the OGD medium was replaced with a standard culture medium. The plates were then maintained in a humidified incubator at 37 °C for 48 h. The control groups were maintained under normoxic conditions for the entire duration of the experiment. OGD and control normoxic cultures were then treated with EVs, which were suspended in sterile PBS and added to the culture medium at a final concentration of 2×10^7 EVs /170.000 cells. The vehicle group received an equivalent volume of PBS. The treatment lasted for 30 h, during which the cultures were maintained under standard conditions in a humidified incubator at 37 °C. The medium containing EVs was not refreshed during this period to maintain a stable exposure.

The expression of the pro-inflammatory marker CD86 and the anti-inflammatory marker CD206 by microglia (Iba-1^+) was evaluated using immunofluorescence. Briefly, cells were fixed with 4 % PFA for 15 min, and then incubated with the following primary antibodies at 4 °C overnight: goat anti-Iba-1 (1:400); rabbit anti-CD86 (1:400), rabbit anti-CD206 (1:400). The secondary antibodies used were Alexa Fluor 488 (1:500) and AlexaFluor 546 (1:500). The secondary antibodies were incubated for 1 h at RT. Cell nuclei were counterstained with DAPI (0.5 μg/ml for 10 min). Images were acquired at 20× magnification using a Nikon A1 MP confocal system (Nikon, Tokyo, Japan). Three randomly selected ROI (1024 × 1024) were taken from each coverslip ($n = 6$ coverslips/condition), and at least two independent experiments were performed.

Primary cortical neurons from embryonic (E17-E19) C57BL/6 mouse brains were prepared according to standard procedures. After brain dissection, the cortical tissues were incubated for 10 min at 37 °C in trypsin-EDTA solution (0.025 %/0.01 % *w/v*; Biochrom AG, Berlin, Germany) in 1 × PBS. The tissues were then mechanically dissociated at RT using a pipette. The cell suspension was harvested and centrifuged at 600 ×*g* for 5 min. The pellet was resuspended in minimum essential medium (MEM, Biochrom AG, Berlin, Germany) containing 5 % fetal bovine serum, 5 % horse serum, 2 mM glutamine, 1 % penicillin-streptomycin antibiotic mixture (Sigma-Aldrich, St. Louis, MO, USA), and 25 mM glucose. Finally, the cells were plated on poly-L-lysine (0.1 mg/ml; Sigma-Aldrich, St. Louis, MO, USA)-pre-coated wells. After 24 h, on day 1 in vitro (DIV1), medium was replaced with Neurobasal (Gibco, Thermo Fisher Scientific, Waltham, MA, USA) supplemented with 2 % B27 (Gibco, Thermo Fisher Scientific, Waltham, MA, USA), 0.5 % Glutamax (Invitrogen, Waltham, MA, USA) and 0.1 % penicillin-streptomycin (Invitrogen, Waltham, MA, USA). After 72 h, at DIV4, the medium was replaced with a glutamine-free medium. The neuronal cultures used were ~ 90 % pure, as assessed by β3-Tubulin (1:500) and MAP2 (1:500) immunoreactivity.

At DIV 11, neuronal cultures were subjected to OGD for 1 h using the same hypoxic chamber and glucose-free DMEM (Gibco, Thermo Fisher Scientific, Waltham, MA, USA, cat. Number 11966–025) described for microglial cultures. After OGD, the cells were returned to normoxic conditions and reperfused with complete Neurobasal medium for 24 h. Control cultures were maintained under normoxic conditions. Twenty-four hours after reperfusion, the cultures were treated with EVs (2×10^7 EV per 170.000 cells, suspended in PBS) or vehicle, as previously described. The EV-containing medium was not changed for 24 h to ensure continuous exposure.

Apoptosis was evaluated using the apoptosis bromodeoxyuridine terminal deoxynucleotidyl transferase dUTP nick end labeling (APO-BrdU TUNEL) assay kit (Invitrogen, Waltham, MA, USA, #A23210) according to the manufacturer's instructions, as previously described (Podda et al., 2014). Briefly, DNA strand breaks in apoptotic cells were labeled with BrdU using terminal deoxynucleotidyl transferase. Apoptotic cells were identified immunocytochemically using anti-BrdU antibody labeling with Alexa Fluor 488 dye, and cell nuclei were identified by propidium iodide/RNase staining. The percentage of BrdU-positive cells was calculated relative to the total number of nuclei. Two-dimensional images for immunofluorescence and TUNEL were acquired at 20× magnification using a Nikon A1 MP confocal system (Nikon, Tokyo, Japan). For each condition, at least four randomly

selected ROIs (1024 × 1024 pixels) per coverslip were acquired ($n = 4$ coverslips/condition), and two independent experiments were performed.

2.9. Statistical analysis

Sample sizes were chosen with adequate statistical power (0.8) according to the results of prior pilot datasets or studies, including ours, using similar methods or paradigms. Analyses were performed using the SigmaPlot 14.0 software. The results are presented as the mean ± SEM. The experimenters were blinded to the group and outcome assignments. Data were first tested for equal variance and normality (Shapiro-Wilk test), and then the appropriate statistical tests were chosen. All statistical tests were 2-tailed and a P value <0.05 was considered statistically significant.

Two-way repeated measures (RM) ANOVA (repetition factor, time) followed by Bonferroni *post-hoc* tests were used to analyze the behavioral data and microglial morphological parameters. Student's *t*-test was used to compare infarct volume, immunofluorescence, and Western blotting data between the vehicle and EV-treated groups. The Mann-Whitney *U* test was used for ELISA data. Two-way ANOVA (treatment × condition) followed by Bonferroni *post-hoc* test was used for in vitro data. The statistical tests used are specified in the Results section and figure legends.

3. Results

3.1. EVs administered intranasally reach the peri-infarct area

First, EVs were isolated from the culture media of human BM-MSCs and were characterized based on their molecular, dimensional, and morphological properties. They exhibited EV-specific markers such as Alix, HSP70, CD9, and CD81, with a size distribution peaking at approximately 100–130 nm (Fig. 2A,B and Supplementary Fig. 1), and displayed the typical shape observed under transmission electron microscopy (Fig. 2C). Importantly, the non-EV marker GM130 was absent in the EV preparations, confirming the removal of contamination from cellular debris, other organelles and compartments.

We labeled BM-MSC-derived EVs with a fluorescent marker to evaluate their biodistribution in the brains of stroke mice. In particular, the animals received a single dose of 1×10^9 ExoGlow™-labeled EVs and were sacrificed 6 h later to evaluate the EV distribution in the brain. Immunofluorescence analysis revealed the presence of EVs in the peri-infarct area, which is characterized by a high density of reactive astrocytes ($GFAP^+$ cells, Fig. 2D).

3.2. EVs promote recovery of several aspects of forelimb motor function

To assess the effects of EV treatment on stroke recovery, we evaluated several aspects of motor function by using a battery of motor tests. As expected, in the cylinder test, the percentage of touches with the preferred paw was significantly reduced 48 h after stroke in both vehicle- and EV-treated mice (vehicle [$n = 13$ mice], 40.75 ± 1.95 % vs. 64.82 ± 1.92 % at baseline; $P < 0.0001$; EV [n = 13 mice], 40.50 ± 1.91 % vs. 60.08 ± 1.95 % at baseline; P < 0.0001; two-way RM ANOVA, Bonferroni *post-hoc*, Fig. 3A). Notably, in EV-treated mice, the placements of the impaired paw increased from the first week post-stroke, and at 4 weeks, it reached a score that was not significantly different from the baseline (59.94 ± 2.53 %; $P = 1$ vs. baseline; Fig. 3A). Instead, at the same time point, vehicle-treated mice still exhibited a statistically significant impairment (49.75 ± 3.17; $P < 0.0001$ vs. baseline; $P = 0.02$ vs. EV-treated mice; Fig. 3A).

We then assessed motor coordination and paw placement accuracy using the grid-walking test. Forty-eight hours post-stroke all mice exhibited a significant increase in the percentage of foot faults in the forelimb contralateral to the damaged motor cortex compared with their pre-stroke values (P < 0.0001 48 h post-stroke vs. baseline for both groups; n = 13 mice/group; Fig. 3B). Results obtained during the

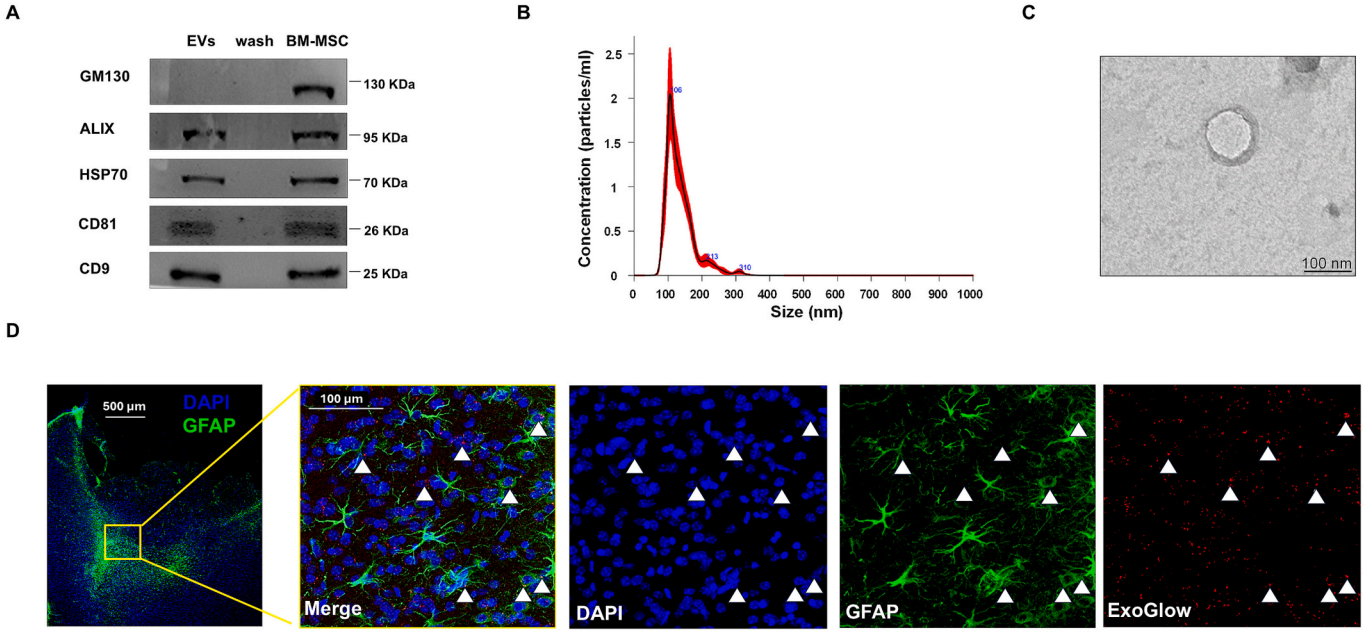

Fig. 2. Intranasal administration of human BM-MSC EVs allows reaching the peri-infarct cortical area. (A) Representative images of immunoblot analysis of proteins extracted from human BM-MSC EVs (EV lysates) and BM-MSC cells (total lysates). The Wash" lane represents the negative control. Alix, HSP70, CD9, and CD81 are EV markers, whereas GM130 is a cellular contamination marker. (B) Nanoparticle tracking analysis spectrum showing the size distribution curve of BM-MSC EVs (C). Transmission electron microscopy image of EV isolated from the human BM-MSC medium. (D) Confocal images of the cortical peri-infarct area of mice intranasally treated with BM-MSC EVs labeled with a fluorescent dye (Exo-Glow, red) and immunostained for GFAP (green). The cell nuclei were counterstained with DAPI (blue). White arrows indicate cell-internalized EVs. (For interpretation of the references to colour in this figure legend, the reader is referred to the web version of this article.)

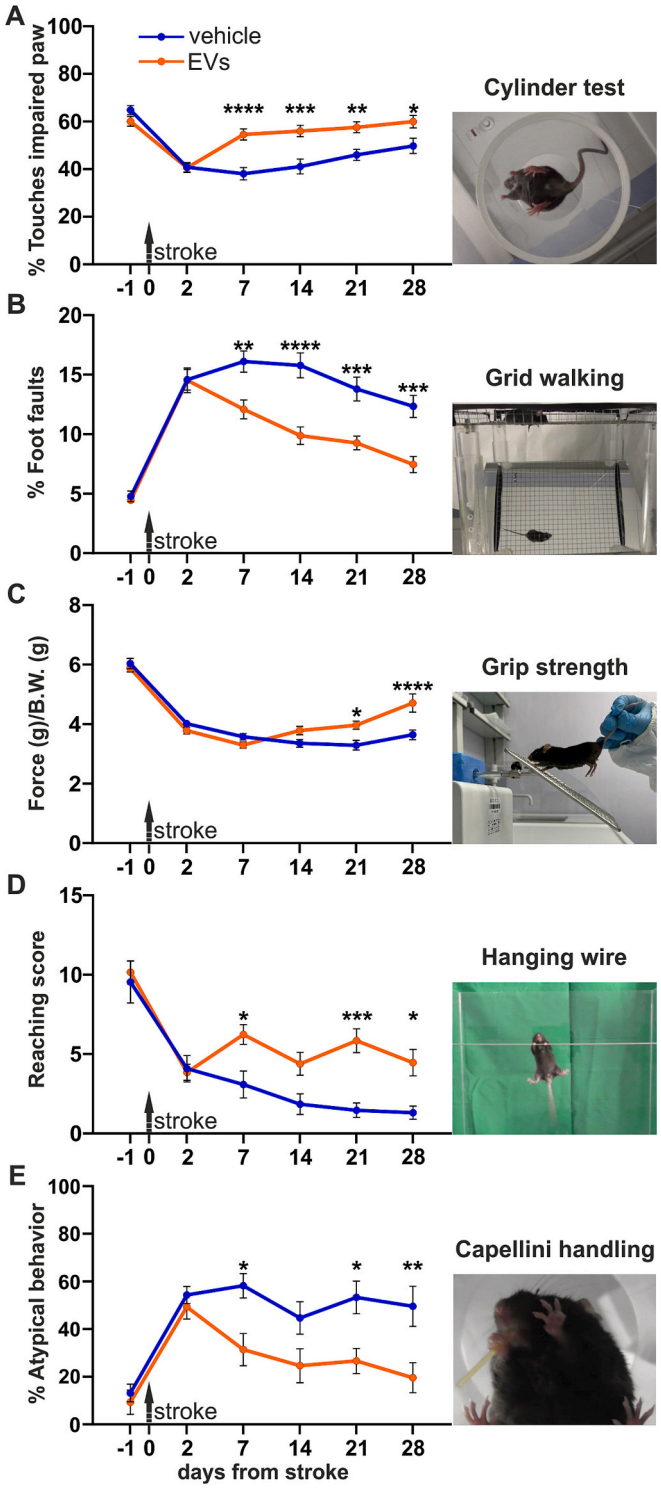

Fig. 3. EV treatment promotes post-stroke functional recovery in mice. Time courses of stroke recovery show that mice treated with EVs show better performance compared to mice treated with vehicle in the cylinder (A), grid walking (B), grip strength (C), hanging wire (D), and capellini handling (E) tests. Representative photographs of mice performing different motor tests are also presented. Thirteen mice per group performed all tests except for the capellini handling, due to the exclusion of four EV and two vehicle mice that did not satisfy the inclusion criteria for this test. Data are expressed as mean ± SEM. $P < 0.05$; *$P < 0.01$; ***$P < 0.001$; ****$P < 0.0001$; EVs vs. vehicle; two-way RM ANOVA Bonferroni *post-hoc* (A: $F_{5,120} = 12.21$, $P < 0.0001$; B: $F_{5,120} = 8.410$, $P < 0.0001$; C: $F_{5,120} = 12.21$, $P < 0.0001$; D: $F_{5,120} = 4.088$, $P < 0.0018$; E: $F_{5,89} = 4.006$, $P = 0.0025$).

recovery period showed that EV mice performed significantly better than vehicle mice from the first week after stroke (main factor, treatment: $F_{1,24} = 15.67$; $P = 0.0006$; two-way RM ANOVA). Four weeks after stroke, the percentage of foot faults was 7.45 ± 0.68 in EV mice vs. 12.34 ± 0.93 in vehicle mice ($P = 0.0002$; Bonferroni *post-hoc*).

Grip strength is an important measure of arm function in stroke patients; therefore, it was evaluated in our experimental model. Mice treated with EVs showed higher grip strength than vehicle-treated mice in the last two weeks of treatment. Specifically, 3 weeks after stroke, forelimb force [(g)/body weight (g)] in EV-treated mice was 3.96 ± 0.13 vs. 3.29 ± 0.16 in vehicle-treated mice (n = 13/each group, $P = 0.018$) and, at 4 weeks, it was 4.71 ± 0.30 vs. 3.64 ± 0.16, respectively ($P < 0.0001$; two-way RM ANOVA, Bonferroni *post-hoc* Fig. 3C).

Similar results were obtained in the hanging wire test, which also relies on the forelimb grip force. Indeed, mice treated with EVs showed significantly higher reaching scores compared to vehicle-treated mice [n = 13/group] at the 4 week-follow up (4.46 ± 0.83 vs. 1.31 ± 0.41 in vehicle-treated mice; $P = 0.02$; two-way RM ANOVA, Bonferroni *post-hoc;* Fig. 3D).

Skilled forepaw ability was also tested using the Capellini handling test. Results showed that EV-treated mice ($n = 9$) performed significantly better than vehicle-treated mice ($n = 11$), as revealed by a decreased percentage of the time spent performing atypical behaviors, namely, symmetrical hold, one paw, and eating from the middle (main factor, treatment: $F_{1,18} = 7.82$; $P = 0.01$; two-way RM ANOVA; Fig. 3E).

Taken together, the results of the functional assessments demonstrated that intranasal administration of human BM-MSC-derived EVs significantly rescued forelimb post-stroke deficits in different motor domains.

3.3. EV treatment reduces infarct size and promotes neuronal survival

Next, we investigated the impact of EV treatment at tissue level and possible mechanisms underlying the effects of EV on motor function recovery. At the end of the last behavioral testing, mice were transcardially perfused, and their brains were processed for histochemical analysis.

Notably, histopathological assessment revealed that infarct volume was reduced in EV-treated mice compared to vehicle-treated mice (infarct volume: 0.49 mm^3 vs. 1.04 mm^3 EV vs. vehicle: $P = 0.03$; $n = 5$ mice/group; Student's *t*-test; Fig. 4A,B). Strikingly, the lesion was almost completely healed in the brains of EV-treated mice. Immunofluorescence staining with the neuronal marker NeuN in the peri-infarct area also showed that the percentage of NeuN-positive cells over the total number of DAPI (i.e., nuclear marker)-positive cells was greater in EV mice than in vehicle-treated mice (88.6 ± 3.17 % vs. 60.8 ± 7.85 %; $P = 0.002$; Student's *t*-test; 3 mice/group; Fig. 4C,D and Supplementary Fig. 2 A), likely indicating decreased secondary neuronal cell death following EV treatment.

3.4. EV treatment attenuates astrogliosis and glial scar formation and dampens brain immune response

Astrocytes and microglia are known to react to ischemic insults, being particularly involved in the acute brain immune response and subsequent chronic glial scar formation, which hinders neural regeneration in the peri-infarct area, worsening functional recovery. Brain sections obtained from mice sacrificed 31 days after stroke were processed for GFAP (glial marker) or Iba-1 (microglia/macrophage marker) staining and counterstained with the nuclear marker DAPI.

GFAP staining showed reduced glial scar formation in mice treated with EVs, as revealed by decreased glial scar area and thickness compared to mice treated with vehicle (area: 0.109 ± 0.019 mm^2 vs. 0.245 ± 0.024 mm^2 in vehicle-treated mice; $P = 0.011$; width: 264.46 ± 37.90 μm vs. 476.69 ± 62.036 μm in vehicle-treated mice; $P = 0.04$; Student's *t*-test; $n = 18$ ROIs, 3 mice/group; Fig. 5A-D).

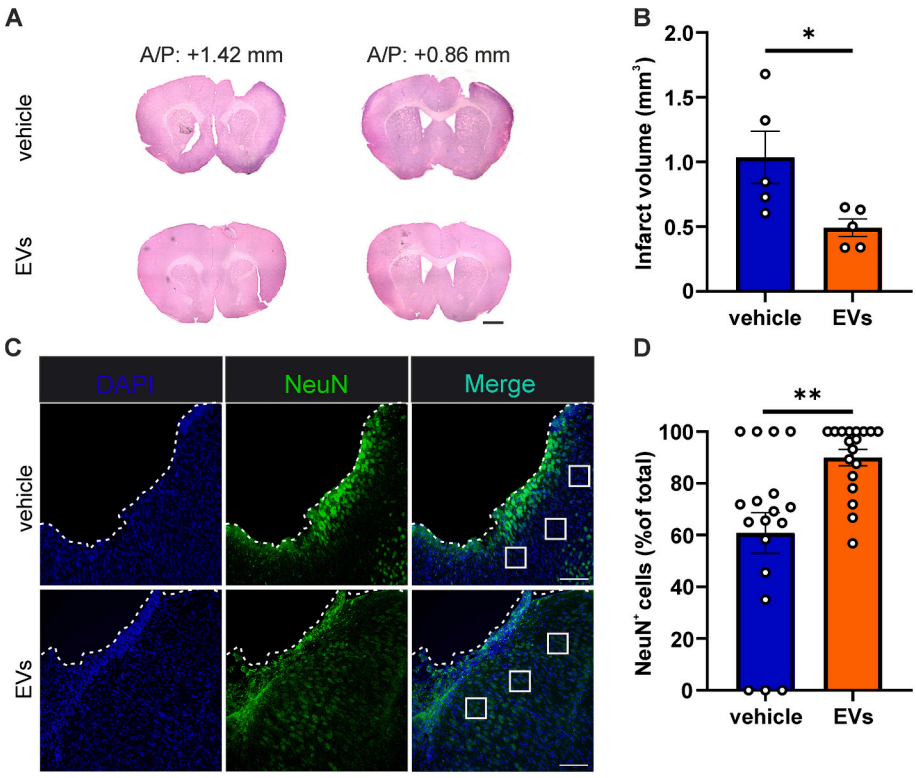

Fig. 4. EVs promote brain tissue repair. (A) Representative Hematoxylin-Eosin-stained coronal brain sections (A/P: anterior-posterior bregma coordinates in mm) and bar graphs (B) show that at the end of 4-week-treatment, the infarct volume was significantly reduced in mice treated with EVs compared to vehicle-treated mice ($n = 5$ mice/group). (C) Representative immunofluorescence labeling of the neuronal marker NeuN (green), positive cells over the total number of cells labeled with the nuclear marker DAPI. The dotted lines demarcate the boundaries of the infarct region. (D) Bar graphs show an increased percentage of neurons in the peri-infarct area of mice treated with EVs compared with vehicle-treated mice ($n = 18$ ROI/group: 3 ROIs/section, 2 sections/mouse, $n = 3$ mice/group). Scale bars: in A, 500 μm; in C, 100 μm. Data are expressed as mean ± SEM. P < 0.05; *P < 0.01; Student's *t*-test. (For interpretation of the references to colour in this figure legend, the reader is referred to the web version of this article.)

In addition, the percentage of GFAP$^+$/DAPI$^+$ cells in the peri-scar area was lower in EV-treated mice than in vehicle-treated mice (56.96 ± 6.46 % vs. 75.35 ± 3.01 %; $P = 0.021$; Student's t-test; n = 18 ROIs, 3 mice/group; Fig. 5E, Supplementary Fig. 2B), further supporting the reduction of astrogliosis following EV treatment.

We then quantified the percentage of Iba-1$^+$/DAPI$^+$ cells in the peri-infarct area that, similar to what we observed for the GFAP staining, was decreased in mice treated with EVs compared to vehicle-treated mice (44.40 ± 3.28 % vs. 54.07 ± 3.04 %; $P = 0.04$; Student's t-test; n = 18 ROIs, 3 mice/group; Fig. 6A and Supplementary Fig. 2C), showing a reduction in microglial activation.

As microglia are early players that rapidly respond to focal lesions by immediately increasing their number, we measured Iba-1$^+$/DAPI$^+$ cells in mice sacrificed 1 week after stroke. In EV-treated mice the percentage of Iba-1$^+$/DAPI$^+$ cells was significantly lower than in vehicle-treated mice (59.98 ± 2.90 % vs. 74.38 ± 2.95 %; $P = 0.001$; Student's t-test; $n = 3$ mice/group; Fig. 6B and Supplementary Fig. 2D).

Activated microglia undergo not only proliferation, but also a morphological shift, transitioning from a resting ramified shape to an activated amoeboid shape, ultimately resulting in complete phagocytic transformation (Morrison and Filosa, 2013). Therefore, we studied Iba-1$^+$/DAPI$^+$ cells to determine their stage along this transformation continuum by examining their morphology at both 7 and 31 days post-stroke (n = 3 mice/group; $n = 10$ cells/mouse; Fig. 6C-E). One week after stroke, the Iba-1$^+$/DAPI$^+$ cells of EV mice exhibited a greater number of branches (161.97 ± 16.90 vs. 102.90 ± 9.97, $P = 0.04$, Fig. 6C,E) and arborization domains (1.17 ± 0.13 mm^2 vs. 0.66 ± 0.10 mm^2, $P = 0.02$, Fig. 6E) than those of the vehicle group. This was associated with a significant decrease in both the soma area (0.0516 ± 0.0018 mm^2 vs. 0.0648 ± 0.0040 mm^2, P = 0.04, Fig. 6E) and morphological index, that is, the soma area/arborization area ratio (0.0472 ± 0.0061 vs. 0.1087 ± 0.0167, $P = 0.006$, Fig. 6E). Four weeks post-stroke, we found a significantly higher number of branches in microglia from EV mice than in the vehicle group (279.20 ± 13.44 vs. 208.42 ± 15.89, P = 0.02, two-way RM ANOVA, Bonferroni *post-hoc*; Fig. 6D,E) with no significant alterations in the other three morphological parameters studied (Fig. 6E).

Given that EVs exerted a more pronounced effect on microglial morphology at an early time point, we further investigated the impact of our treatment on the neuroinflammatory response by measuring the levels of the anti-inflammatory cytokines IL-10 and IL-13 and the pro-inflammatory cytokines IL-1β, IL-6, and TNF-α in brain extracts of the peri-infarct area collected 3 days after stroke. Our ELISA assays showed a significant increase in IL-10 and IL-13 levels in EV-treated mice compared to vehicle-treated mice (IL-10: 110.5 ± 15.22 pg/mg vs. 62.57 ± 4.10 pg/mg; $n = 9$ mice/group; $P = 0.0003$; IL-13: 1204.6 ± 304.75 pg/mg vs. 736.5 ± 144.67 pg/mg; P = 0.04; Mann-Whitney test; $n = 6$ mice/group; Fig. 7A). This was paralleled by a significant reduction of IL-1β, IL-6 and TNF-α levels in EV-treated mice (IL-1β: 22.44 ± 1.43 pg/mg vs. 44.02 ± 9.45 pg/mg, P = 0.04; n = 9 mice/group; IL-6: 42.32 ± 10.95 pg/mg vs. 78.67 ± 10.73 pg/mg, $P = 0.026$; TNF-α: 27.73 ± 4.97 pg/mg vs. 64.40 ± 17.38 pg/mg, P = 0.026; Mann-Whitney test; n = 6 mice/group; Fig. 7A). Collectively, our findings suggest that EV treatment mitigates the brain immune response during the subacute phase following stroke.

NLRP3 inflammasome activation has been implicated in the development and progression of ischemic stroke, contributing to neuroinflammation and secondary cell death (Wang et al., 2022; Xu et al., 2025). Therefore, we evaluated the effects of EVs on the expression of NLRP3 and its downstream signaling cascade involving activated

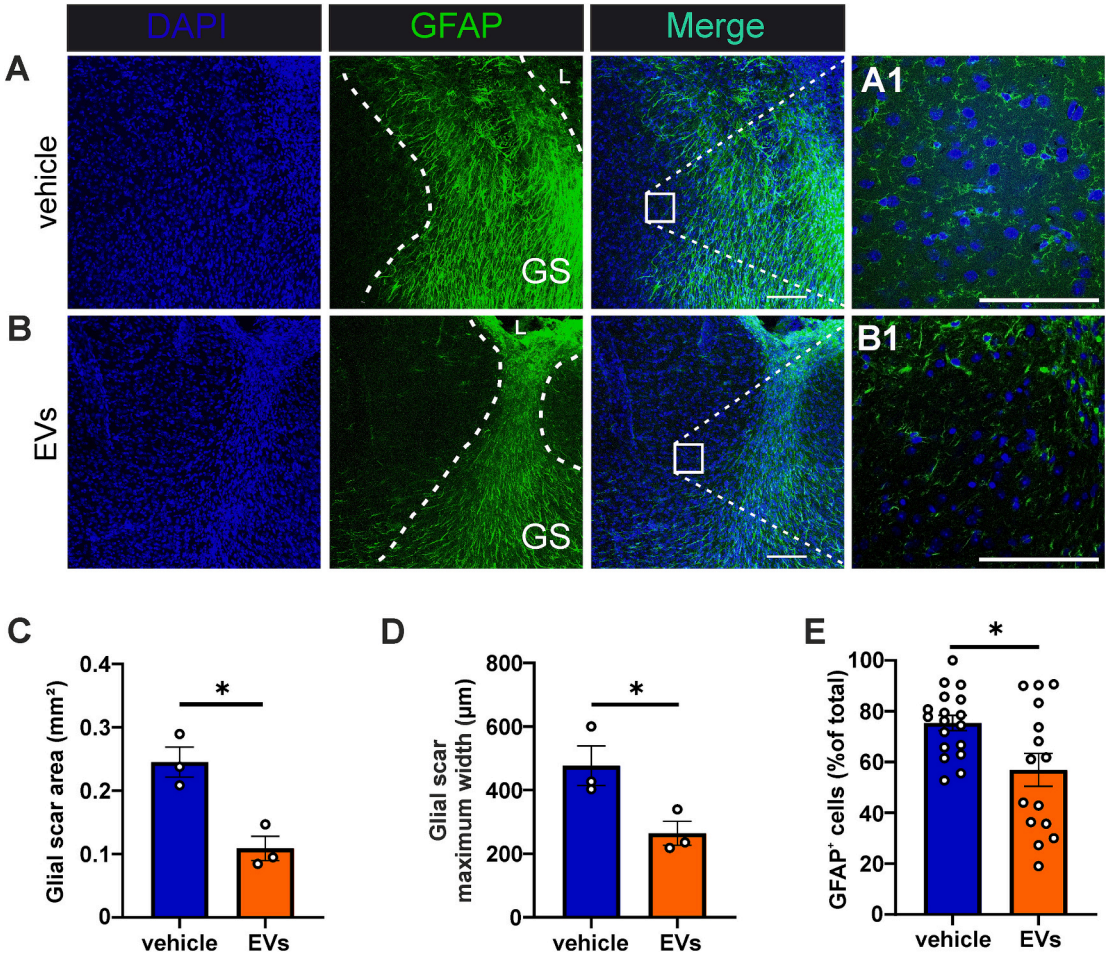

Fig. 5. Astrogliosis and glial scar formation are reduced following EV treatment. Immunostaining of GFAP (green) with DAPI counterstaining (blue) for cell nuclei in representative sections from vehicle (A) and EV mice (B) 31 days after stroke. Dashed lines indicate the margins of the glial scar (GS). Scale bar: 100 µm. A1 and B1 show high-magnification images (60×) of the ROI acquired in the peri-scar regions delineated with white boxes in panels A and B. Scale bar: 100 µm. L: ischemic lesion. Bar graphs show that mice treated with EVs (n = 3/group) displayed reduced glial scar area (C) and thickness (D), together with a reduced number of $GFAP^+$ cells in the peri-scar region (E) compared to vehicle-treated mice (n = 3; 6 ROI each). Data are expressed as mean ± SEM. *P < 0.05; Student's t-test. (For interpretation of the references to colour in this figure legend, the reader is referred to the web version of this article.)

Cleaved Caspase-1. Compared to vehicle-treated mice ($n = 4$), EV mice (n = 4) showed decreased expression of NLRP3 (−24 %; $P = 0.031$; Student's *t*-test; Fig. 7B and Supplementary Fig. 3) and significantly reduced levels of Cleaved Caspase-1 (−74 %; $P = 0.013$; Student's t-test; Fig. 7C and Supplementary Fig. 3).

3.5. *EVs rescue the pro-inflammatory response of microglia and promote neuronal survival in vitro following ischemia by OGD*

To specifically address the contribution of EVs in modulating microglial response and promoting neuronal survival, we performed in vitro experiments on microglial and neuronal cell cultures, respectively, subjected to ischemia by OGD, followed by EV or vehicle treatment (Fig. 8A).

In particular, we characterized the pro- or anti-inflammatory phenotype of microglial cell culture by assessing the expression of the pro-inflammatory marker CD86 and the anti-inflammatory marker CD206 (Fig. 8B and Supplementary Fig. 4B). The results demonstrated that after the OGD protocol, Iba-1^+ cells treated with the vehicle exhibited increased expression of the pro-inflammatory marker CD86 (Fig. 8B) and decreased expression of the anti-inflammatory marker, CD206 (Fig. 8C) compared to control culture maintained in normoxic condition (CD86: 61.5 ± 3.87 % OGD vehicle vs. 47.94 ± 0.75 % control vehicle; $P = 0.0016$; CD206: 38.82 ± 3.9 % OGD vehicle vs. 63.35 ± 3.47 % control vehicle; $P = 0.0009$; two-way ANOVA, Bonferroni *post-hoc;* Fig. 8B,C). Notably, treatment with EVs significantly mitigated the microglial inflammatory response after OGD (main factor treatment: $F_{1,5} = 112.2$; $P = 0.0001$; treatment × condition interaction: $F_{1,5} = 129.6$; $P < 0.0001$; two-way ANOVA). In particular, EVs decreased the expression of CD86 (34.46 ± 2.54 %; P = 0.0001 vs. OGD vehicle; Fig. 8B) while increasing the expression of CD206 (60.03 ± 3.73 %; $P = 0.0003$ vs. ODG vehicle; Fig. 8C) to levels that were not significantly different from those observed in control normoxic condition as for CD206 expression ($P = 0.24$ vs. control vehicle) and even lower than those of control cells as for CD86 ($P = 0.009$ vs. control vehicle). Consistent with the data obtained in vivo, these findings indicate that EVs attenuate the post-ischemic inflammatory response in microglia.

Neuronal apoptosis was assessed using the TUNEL assay in primary cortical neuron cultures subjected to OGD, followed by treatment with either EVs or vehicle (Fig. 9A Supplementary Fig. 5). Quantitative analysis revealed a significant increase in the percentage of $TUNEL^+$ cells in the OGD vehicle group compared to that in the control vehicle group (33.08 ± 2.363 % vs. 14.85 ± 2.03 %, $P = 0.0057$; two-way ANOVA, Bonferroni *post-hoc;* Fig. 9B,C), indicating a marked apoptotic response following OGD. Treatment with EVs significantly reduced OGD-induced neuronal apoptosis ($TUNEL^+$ cells: 14.58 ± 0.80 %; $P = 0.0054$ vs. OGD vehicle; two-way ANOVA, Bonferroni *post-hoc*), restoring the percentage of $TUNEL^+$ cells to values close to those of

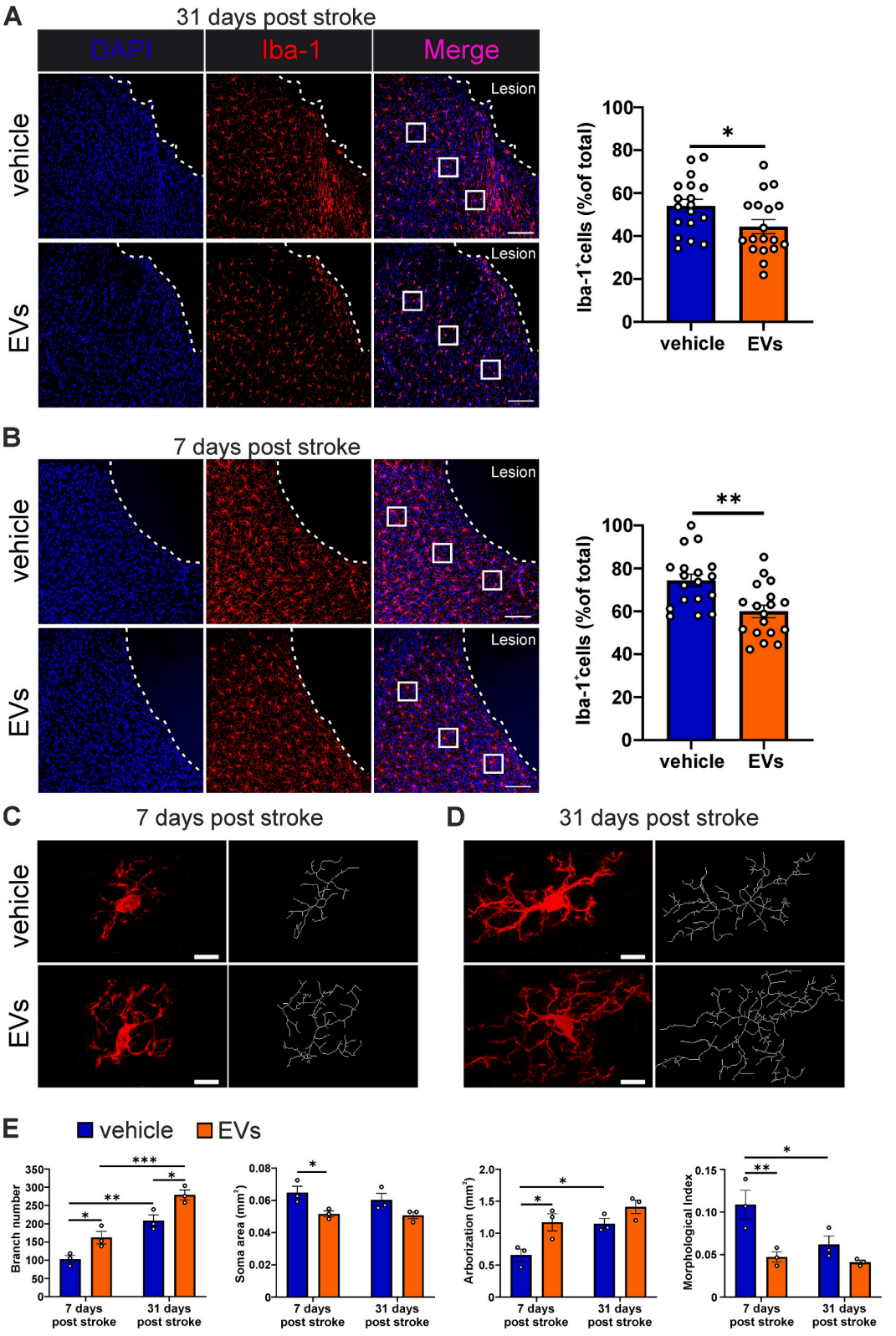

Fig. 6. EVs downregulate the activation of microglia. Representative immunofluorescence labeling of Iba-1 positive cells (red) at 31 days (A) and 7 days post-stroke (B) in mice treated with EVs or vehicle. Cell nuclei were counterstained with DAPI (blue). Scale bars in A and B: 100 μm. Bar graphs show a decreased percentage of Iba-1^{+} cells in the peri-infarct area of mice treated with EVs compared with vehicle-treated mice (n = 18 ROI/group: 3 ROIs/section, 2 section/mouse, n = 3 mice/group) at 31 days (A) and 7 days (B) post-stroke. The ROI position is indicated by white boxes. P < 0.05; *P < 0.01; Student's t-test. (C,D) High-magnification images (60×) of representative Iba-1^{+} microglia and their respective skeletonized images at 7 (C) and 31 days (D) post-stroke in the peri-infarct area of EV- or vehicle-treated mice. Scale bars in C and D: 10 μm. (E) Bar graphs showing the results of morphological analysis regarding the number of branches, soma area, arborization area, and morphological index at 7 and 31 days in the two experimental groups (n = 3 mice/group; *n* = 10 cells/mouse). P < 0.05; *P < 0.01; ***P < 0.001; two-way RM ANOVA, Bonferroni *post-hoc* (branches: $F_{1,8} = 0.1672$, $P = 0.69$; soma area: $F_{1,8} = 0.33$, $P = 0.58$; arborization area: $F_{1,8} = 1.396$, $P = 0.2714$; morphological index: $F_{1,8} = 3.936$, $P = 0.082$). (For interpretation of the references to colour in this figure legend, the reader is referred to the web version of this article.)

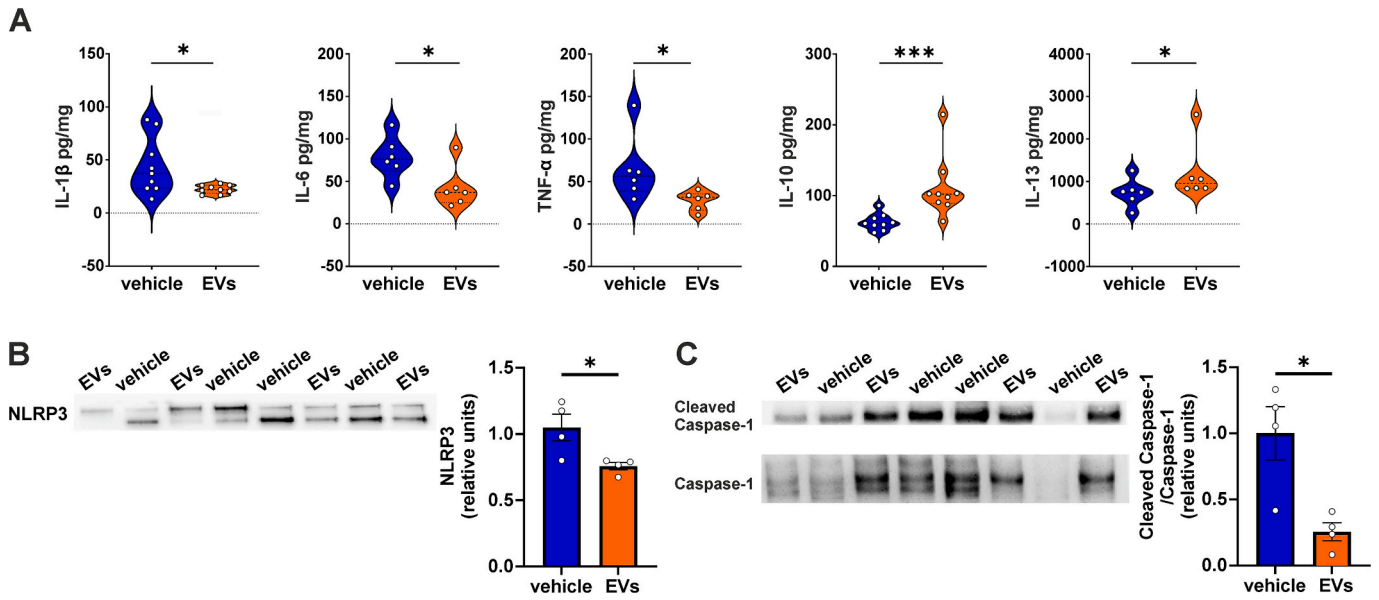

Fig. 7. EVs promote anti-inflammatory responses. (A) Violin plots report results from ELISA showing that EV-treated mice had reduced levels of the pro-inflammatory IL-1β, IL-6, and TNF-α and higher levels of the anti-inflammatory cytokines IL-10 and IL-13 and compared to vehicle-treated mice. Values for each mouse are shown by white circles, and the mean value is indicated by the thick dotted line. $P < 0.05$; $^{**}P < 0.001$; Shapiro-Wilk test not passed, non-parametric Mann-Whitney test. (B,C) Representative Western immunoblots and band densitometry, normalized to total protein level (Ponceau S staining), revealing decreased expression of NLRP3 (B) and Cleaved Caspase-1 (C) in the peri-infarct tissue of mice treated with EVs at 3 days post-stroke. NRLP3 levels were quantified by summing the densitometric values of the two bands corresponding to full-length NLRP3 (upper band) and its processed form (lower band), according to the manufacturer's specifications and literature (Coll et al., 2015). Data are expressed as mean ± SEM. $^{*}P < 0.05$; Student's t-test.

normoxic cultures ($P > 0.99$). Under normoxic conditions, the percentage of apoptotic neurons treated with EVs was not significantly different from that observed in vehicle-treated cultures (13.59 ± 1.44 % vs. 14.85 ± 2.03 %; two-way ANOVA; $P > 0.99$; Fig. 9B), supporting the effects of EVs in the context of the ischemia-triggered insult.

These results indicate an anti-apoptotic effect of EVs, which strongly supports their effects observed at the tissue level, namely, reduced infarct size and neuronal cell death at the end of treatment.

3.6. Human BM-MSC-derived EVs contain detectable levels of BDNF and anti-inflammatory cytokines

To gain insight into the possible molecular determinants of the beneficial effects of EVs observed at both tissue and cell levels, we analyzed the EV cargo to identify neuroprotective and bioactive molecules. Quantitative ELISA assays revealed detectable amounts of hBDNF, IL-2, IL-4, IL-8, and IL-13 in EV lysates (BDNF average concentration: 36.7 ± 5.2 pg/ml; IL-2 average concentration: 21.9 ± 5.6 pg/ml; IL-4 average concentration: 5.7 ± 0.7 pg/ml; IL-8 average concentration: 5.6 ± 0.4 pg/ml; IL-13 average concentration: 8.3 ± 0.4 pg/ml; $n = 3$ EV independent preparations; Fig. 10). These results confirm that pro-neuroplastic and anti-inflammatory factors, such as BDNF, IL-2, IL-4, IL-8, and IL-13 are packaged within EVs derived from BM-MSCs, supporting their potential role in mediating the neuroprotective effects observed in recipient neurons following ischemic injury.

4. Discussion

Stroke is a major public health issue worldwide, given its high rates of death and disability and the lack of effective pharmacological therapy, except for tissue plasminogen activator, which has limited use owing to its narrow therapeutic window (Bersano and Gatti, 2023).

Our study strongly supports the efficacy of BM-MSC EVs in the treatment of neurological disorders by providing a comprehensive characterization of the positive effects of human BM-MSC EVs in alleviating the adverse effects of cortical stroke at functional, tissue, and molecular levels. This includes uncovering a significant modulation of the brain's immune response, which involves reduced glial scar formation, microglial activation, and pro-inflammatory cytokine expression. Specifically, our findings demonstrate that intranasally administered EVs effectively reach the peri-infarct area, thus delivering their beneficial cargo to the injured brain region and overcoming the major challenges associated with stem cell transplantation or systemic delivery. From a translational perspective, it is noteworthy that the intranasal administration route is non-invasive and does not require the subject's cooperation. This would enable the initiation of a treatment regimen at an early post-stroke phase, specifically 48 h post-stroke, which is a critical period for the initial onset of spontaneous recovery mechanisms (Ding and Zhang, 2021; Longo et al., 2022). Although there are several anatomical and functional differences in the nose-to-brain migratory system between mice and humans, which may limit the translational potential of preclinical studies (Borlongan et al., 2024; Sánchez et al., 2025), recent clinical studies have underscored the promising efficacy of the intranasal route for treating numerous central nervous system diseases (Drath et al., 2025).

Our study provides a detailed assessment of functional recovery by evaluating various aspects of motor function, including forelimb asymmetry, coordination, precise paw placement, force, and skilled forepaw ability. At the 4-week follow-up, mice treated with EVs exhibited significantly better performance than those treated with the vehicle in all tests. Interestingly, in most tests, improvements in deficits among EV-treated mice began one week after stroke, following only two doses of EVs. Performance either remained consistent or further improved over the subsequent three weeks of EV treatment, an effect that was potentially sustained by repeated EV administration. However, we cannot rule out the possibility that treatment administered solely during the first week post-stroke might suffice to yield long-lasting effects. This question will be explored in a follow-up study.

In preclinical studies, the reduction of infarct volume is a standard measure for assessing treatment efficacy, and although debated, it has been advocated as a biological surrogate or auxiliary outcome measure for human ischemic stroke clinical trials (Saver et al., 1999). We found

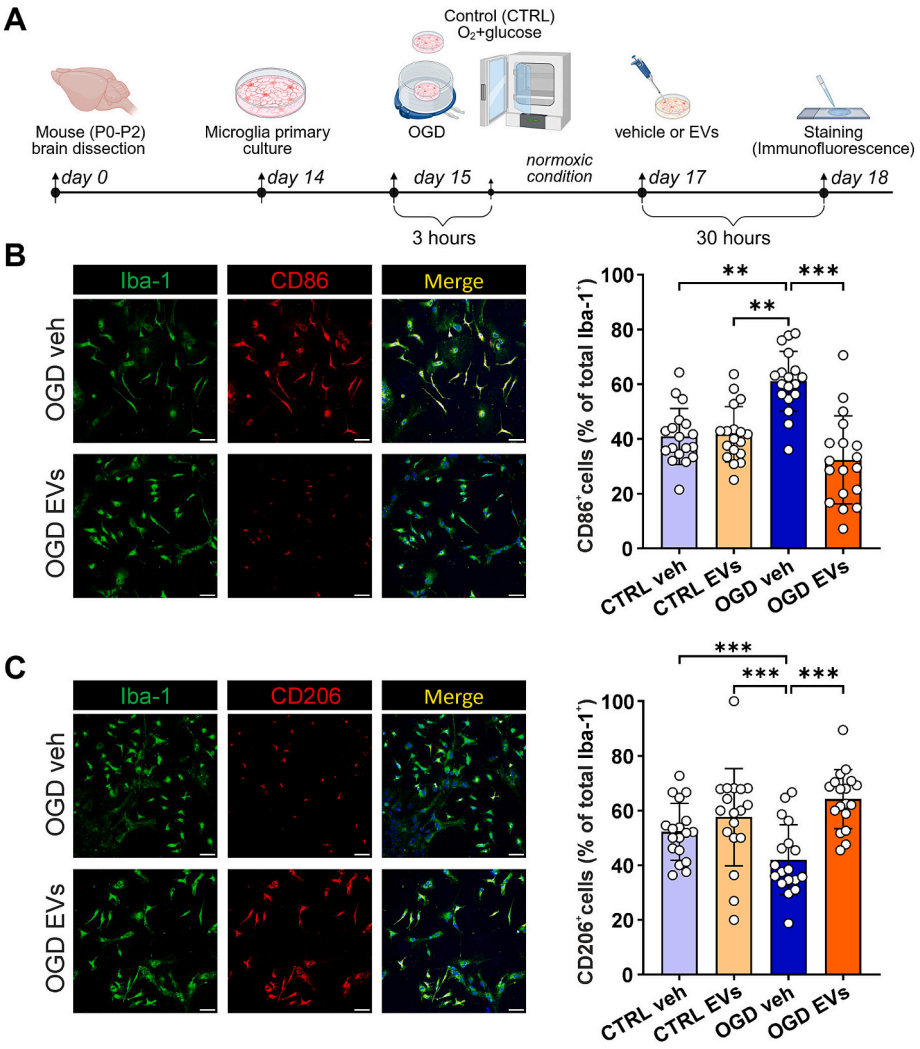

Fig. 8. EVs mitigate neuroinflammatory responses induced by OGD in microglial cell culture. (A) Schematic representation of the OGD protocol and in vitro EV treatment. Representative immunofluorescence images show immunoreactivity for CD86 and Iba-1 (B) and C206 and Iba-1 (C) in OGD glial cultures treated with EV or vehicle. Cell nuclei were counterstained by using DAPI (blue). Scale bars: 50 μm. Bar graphs summarize the results obtained in all experimental groups ($n = 6$ coverslips/group; n = 3 ROIs/coverslip), including the control (CTRL) culture maintained under normoxic conditions (see also Supplementary Fig. 4B). Data were collected from two independent experiments and are expressed as mean ± SEM. $P < 0.005$; *P < 0.001; two-way ANOVA, Bonferroni *post-hoc* (B: $F_{1,5} = 129.6$, P < 0.0001; C: $F_{1,5} = 65.21$, $P = 0.0005$). Panel A was created using Biorender. (For interpretation of the references to colour in this figure legend, the reader is referred to the web version of this article.)

that at the end of EV treatment, mice showed significantly smaller infarct volumes than vehicle-treated mice.

It is noteworthy that, although the photothrombotic stroke model is considered milder than MCAO models, a necrotic core is evident, and there is a substantial loss of neurons in the well-defined peri-infarct area, which experiences astrogliosis and microgliosis phenomena (Sanchez-Bezanilla et al., 2021), both of which play a significant role in stroke and other neuropathological conditions (Berlet et al., 2021).

Mice treated with EVs showed an increased number of neurons in the peri-infarct area compared to vehicle-treated mice, indicating that EVs counteract neuronal loss following an acute insult. The total number of $DAPI^+$ cells was similar in both groups, likely because the reduced number of neurons in the peri-infarct area of vehicle mice was offset by glial cells.

Post-stroke functional improvements and restorative effects have also been reported following transplantation/systemic administration of MSCs in animal models of severe stroke (Ishizaka et al., 2013; Myers et al., 2023). Despite some positive outcomes (Savitz et al., 2011; Steinberg et al., 2018), numerous clinical trials have struggled to successfully translate these results to stroke patients (Detante et al., 2018; Li et al., 2021). The factors potentially contributing to this lack of success include the severity of stroke-induced damage and inadequate cell delivery to the brain (Bang et al., 2016).

Our findings, which demonstrate healing of the injured cortex and significant recovery of motor function in a mouse model of focal ischemia, suggest that intranasal delivery of EVs could be more effective for treating cortical infarcts in clinical settings. Moreover, the success of our protocol may enable the adaptation of dosage for different rodent models, such as rats, and varying severities of stroke to achieve enhanced recovery. Notably, it has been shown that a single intranasal dose of 2.4×10^9 MSC-derived EVs improved neurological function in MCAO when combined with intensive handling, but not when administered alone as a single or multidose approach, which may indicate an insufficient concentration of EVs (Gomez-Galvez et al., 2024). Another recent study conducted in a MCAO stroke model used intranasally administered EVs derived from induced pluripotent stem cells generated from human urine epithelial cells (Zhou et al., 2023). The authors reported more pronounced effects of EVs artificially loaded with BDNF, which is not naturally present in their native EVs, supporting its significant role in stroke recovery (Longo et al., 2022). Notably, we utilized

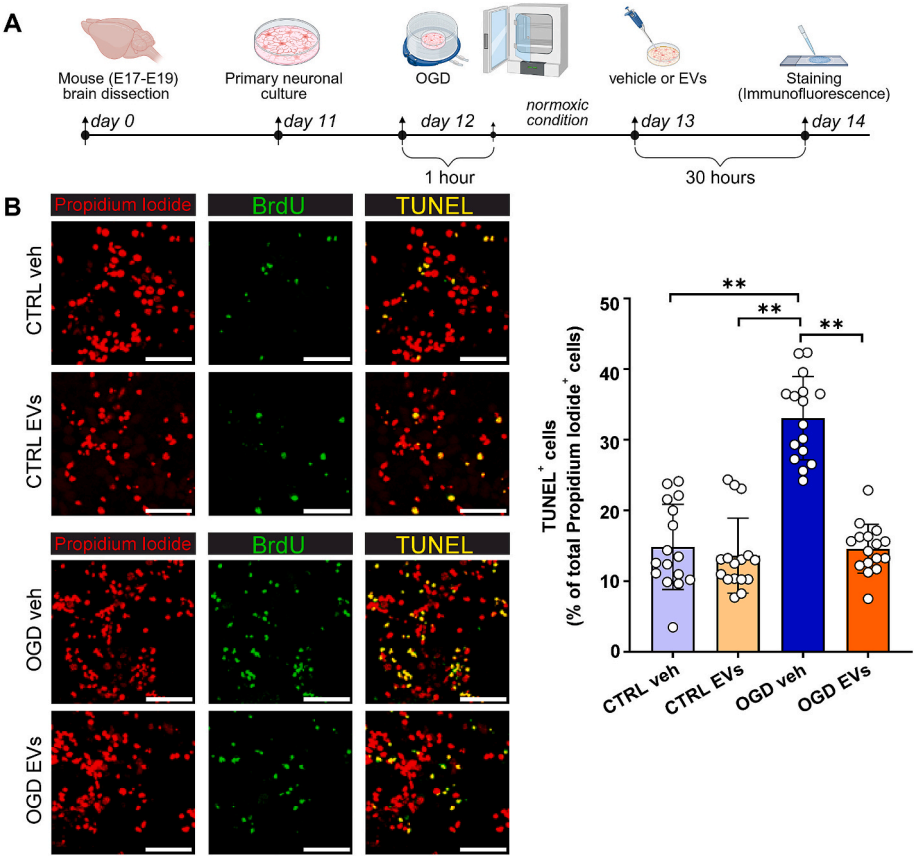

Fig. 9. EVs reduce neuronal apoptosis induced by OGD in cultured cortical neurons. (A) Schematic representation of OGD protocol and in vitro EV treatment. (B) Representative images showing apoptotic TUNEL$^+$ cells (yellow, merged) in neuronal cultures exposed to normoxia (CTRL) or OGD, followed by treatment with EVs or vehicle (veh). Immunostaining for propidium iodide (red) and BrdU (green) is also shown in the figure. Scale bars: 50 μm. (C) Bar graph showing the percentage of apoptotic neurons (TUNEL$^+$ cells, yellow expressed as a percentage of total propidium iodide-positive nuclei) under different experimental conditions ($n = 4$ coverslips/conditions; n = 4 ROIs/coverslip). Data were collected from two independent experiments and are expressed as mean ± SEM. Two-way ANOVA followed by Bonferroni *post-hoc* test; $P < 0.05$, $^{***}P < 0.0001$. Main factor, condition (i.e., OGD or CTRL): $F_{1,3} = 124.4$, $P = 0.0015$; main factor, treatment (i.e., EV or vehicle): $F_{1,3} = 28.86$, $P = 0.012$; condition×treatment interaction: $F_{1,3} = 77.68$, $P = 0.0031$). Panel A was created with Biorender. (For interpretation of the references to colour in this figure legend, the reader is referred to the web version of this article.)

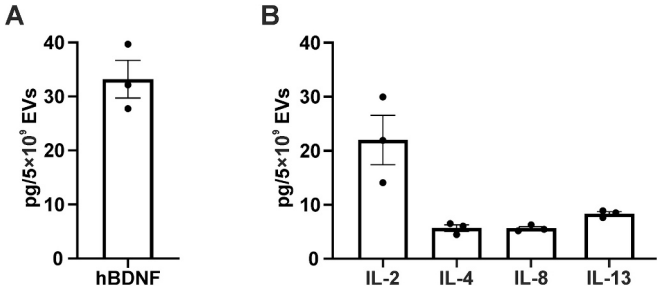

Fig. 10. EVs contain neuroprotective and anti-inflammatory molecules. Bar graphs showing the results of ELISA revealing (A) hBDNF and (B) IL-2, IL-4, IL-8, and IL-13 proteins in EV lysates (n = 3 independent EV preparations). Data are expressed as mean ± SEM.

naïve EVs derived from readily available cell sources (potentially usable in autologous transplantation) containing BDNF, making our approach more translatable to studies on patients affected by stroke or other neurological disorders.

In our photothrombotic model, a significant effect of EV treatment was the consistent reduction in glial scar formation observed four weeks post-stroke. Stroke lesions are known to cause extensive neuronal death, leading to the release of various factors that initiate both glial scar formation and immune response. Almost immediately following an ischemic event, astrocytes and microglia accumulate rapidly around the lesion, increasing the expression of pro-inflammatory cytokines and chemokines that hinder axonal regeneration. During the first week, the scar becomes denser, and by the second week, it matures, forming tight borders between the fibrotic and glial components (Zbesko et al., 2018). Our immunofluorescence analysis showed a significant reduction in astrogliosis at four weeks in mice treated with EVs compared to the control group.

Under normal physiological conditions, astrocytes can maintain microglia in a dormant state. However, under ischemic conditions, the ability of astrocytes to propagate calcium ions over long distances may activate microglia, even far from the infarct area (Nedergaard and Dirnagl, 2005).

Given the crosstalk between these two populations of glial cells (Liu et al., 2011), we focused our analysis on microglia. Immunofluorescence analysis revealed a significant decrease in Iba-1-positive cells in the peri-infarct area of mice treated with EVs for 4 weeks after stroke. While this effect might partly result from the natural healing process, the more pronounced effects observed at one week clearly demonstrate the role of EVs in modulating the microglial response during the subacute phase of stroke. This result prompted us to examine microglial morphology. A substantial body of literature describes how activated microglia undergo proliferation and morphological changes, transitioning from a resting ramified shape to an activated amoeboid shape that can migrate to the lesioned area, where it performs its phagocytic role (Morrison and

Filosa, 2013). In our study, we analyzed four different parameters to determine the activation state of microglial cells, including the branch length and soma area. Our findings indicated that in mice treated with EVs, Iba-1$^+$ cells exhibited a higher number of branches and a concurrent reduction in the soma area, suggesting a shift towards a resting state compared to the vehicle group. These results were supported by in vitro experiments on cultured microglial cells (Iba-1$^+$) exposed to ischemic insult, showing that EVs reversed the pro-inflammatory phenotype, as evidenced by decreased expression of the pro-inflammatory marker CD86 and increased expression of the anti-inflammatory marker CD206, compared to vehicle-treated OGD microglia.

Our data also indicate that downregulation of the neuroinflammatory response in peri-infarct tissue is a mechanism that potentially contributes to the beneficial effects of EV treatment. We observed decreased levels of the pro-inflammatory cytokines IL-1β, IL-6, and TNF-α, which are key components of post-stroke inflammasomes (Kumari et al., 2024), alongside increased levels of the anti-inflammatory cytokines IL-10 and IL-13. These cytokines orchestrate cellular response, including cell survival, anti-apoptotic signaling, and matrix metalloproteinase secretion, which are all crucial for the migration of neural stem cells and cellular rearrangement within the glial scar (Piepke et al., 2021; Chen et al., 2022). Numerous studies have shown that activation of the NLRP3 inflammasome in ischemic stroke exacerbates the inflammatory status, contributing to secondary neuronal cell death in a vicious cycle (Wang et al., 2022; Kumari et al., 2024; Xu et al., 2025). Our findings that EV treatment reduced the levels of the NLRP3 inflammasome and its related pathway, involving the activated form of Caspase-1, namely Cleaved Caspase-1, provide novel insights into the mechanisms mediating the beneficial effect of EVs on stroke recovery. These findings underscore the beneficial impact of EV treatment in preemptively promoting an anti-inflammatory environment for neurons, thereby facilitating a reparative mechanism that mitigates secondary cell death. This resulted in an increased number of neurons in the peri-infarct area, as indicated by our NeuN immunofluorescence assay on brain tissue, corroborated by the TUNEL assay in neuronal cultures exposed to OGD.

The beneficial effects of EVs likely arise from a complex cooperative action involving the activation of anti-inflammatory pathways and enhancement of the production and release of trophic factors by both EVs and injured tissue. Previous studies have demonstrated that BM-MSCs secrete BDNF, glial cell-derived neurotrophic factor, and vascular endothelial growth factor (Doorn et al., 2012; Fu et al., 2017), and anti-inflammatory cytokines, all of which contribute to their therapeutic effects in brain ischemia (Yoo et al., 2013). Notably, our ELISA detected the presence of BDNF and several cytokines, such as IL-2, IL-4, and IL-13, which are involved in neuroprotective and anti-inflammatory effects in brain injuries, including stroke, as demonstrated by the activation of their main downstream pathways in EV-targeted tissues (Gadani et al., 2012; Chen et al., 2022; Zhou et al., 2023; Zhang et al., 2025). A causal link for the role of BDNF in mediating the neuroreparative and anti-inflammatory effects of MSC-EVs was provided by Ahn et al. (2021) using BDNF-knockdown EVs. In particular, the authors showed that the effects of MSC-derived EVs, which significantly attenuate severe intraventricular hemorrhage-induced apoptotic cell death, inflammatory responses, oxidative stress, and astrogliosis, were abolished with BDNF small interfering RNA transfection.

Notably, increased level of the pro-inflammatory cytokine IL-8, which has been reported in human and animal biological fluids following brain trauma, has been shown to promote neuronal survival by stimulating the synthesis of nerve growth factor (Kossmann et al., 1997). Additionally, we cannot rule out the possibility that other bioactive molecules within the EV cargo, such as non-coding RNAs, lipids, and various cytokines—including those analyzed but undetectable, because they are below the quantification limits—may contribute to the neuroprotective effects of human BM-MSC-derived EVs (Dhuria et al., 2010; Moon et al., 2019).

Despite evidence showing the effects of EVs on microglial activation post-ischemia both in vivo and in vitro, the full impact of EVs on neuroinflammation, the exact sources of pro- and anti-inflammatory factors, which may involve microglia, astrocytes, infiltrating macrophages, and lymphocytes, and their subsequent pathways, along with the complex interactions between astrocytes and microglia (Liddelow, 2017) in our model, require further exploration. Future research should also aim to identify neuroinflammation-independent mechanisms activated by EVs that likely involve neuroplasticity, neovascularization, and neurogenesis, potentially aiding the functional recovery observed in stroke mice.

5. Conclusions

In summary, our research significantly contributes to the expanding body of evidence supporting the beneficial effects of EVs derived from human BM-MSC on neurological disorders. It also provides a rationale for translating intranasal delivery of EVs into clinical settings, particularly for cortical stroke rehabilitation. Leveraging the tissue repair and immunomodulatory properties of EVs holds potential as a targeted and effective therapeutic strategy for stroke patients, particularly during the early recovery phase. Future studies should carefully consider factors such as the optimal dosage, timing, and potential combinatory approaches with existing interventions. This pursuit not only holds the potential to identify therapeutic targets aimed at reducing inflammation and promoting post-stroke recovery but also opens a compelling avenue for advancing our understanding of neuroprotective mechanisms following ischemic stroke.

CRediT authorship contribution statement

Saviana Antonella Barbati: Writing – review & editing, Writing – original draft, Methodology, Investigation, Conceptualization. **Chiara D'Amelio:** Methodology, Investigation, Formal analysis. **Chiara Feroleto:** Methodology, Investigation, Formal analysis. **Marta Morotti:** Methodology, Investigation, Formal analysis. **Ida Nifo Sarrapochiello:** Methodology, Investigation. **Francesca Natale:** Methodology, Investigation. **Domenica Donatella Li Puma:** Methodology, Investigation. **Yolanda Gomez-Galvez:** Methodology. **Elena Blanco-Suarez:** Methodology, Conceptualization. **Lorraine Iacovitti:** Conceptualization. **Lucia Leone:** Methodology, Investigation. **Salvatore Fusco:** Writing – review & editing, Supervision, Conceptualization. **Maria Vittoria Podda:** Writing – review & editing, Writing – original draft, Supervision, Project administration, Methodology, Data curation, Conceptualization. **Claudio Grassi:** Writing – review & editing, Project administration, Funding acquisition, Conceptualization.

Funding

Thomas Jefferson University grant (TJU-Stroke Project). Fondazione Policlinico Universitario "A. Gemelli" IRCCS (Ricerca Corrente to C.G).

Declaration of competing interest

The authors declare that they have no known competing financial interests or personal relationships that could have appeared to influence the work reported in this paper.

Acknowledgements

We would like to acknowledge the contribution of "Microscopy" Core Facility G-STeP, Fondazione Policlinico Universitario "A. Gemelli" IRCCS.

Appendix A. Supplementary data

Supplementary data to this article can be found online at https://doi.org/10.1016/j.expneurol.2025.115540.

Data availability

The data supporting the findings of this study are available within the article and from the corresponding authors upon reasonable request.

References

Ahn, S.Y., et al., 2021. Brain-derived neurotropic factor mediates neuroprotection of mesenchymal stem cell-derived extracellular vesicles against severe intraventricular hemorrhage in newborn rats. Stem Cells Transl. Med. 10, 374–384. https://doi.org/10.1002/sctm.20-0301.

Bakreen, A., et al., 2021. Additive behavioral improvement after combined cell therapy and rehabilitation despite long-term microglia presence in stroke rats. Int. J. Mol. Sci. 22, 1512. https://doi.org/10.3390/ijms22041512.

Bang, O.Y., et al., 2016. Adult stem cell therapy for stroke: challenges and progress. J. Stroke 18, 256–266. https://doi.org/10.5853/jos.2016.01263.

Berlet, R., et al., 2021. Combination of stem cells and rehabilitation therapies for ischemic stroke. Biomolecules 11, 1316. https://doi.org/10.3390/biom11091316.

Bersano, A., Gatti, L., 2023. Pathophysiology and treatment of stroke: present status and future perspectives. Int. J. Mol. Sci. 24, 14848. https://doi.org/10.3390/ijms241914848.

Borlongan, C.V., et al., 2024. Nose-to-brain delivery of stem cells in stroke: the role of extracellular vesicles. Stem Cells Transl. Med. 13, 1043–1052. https://doi.org/10.1093/stcltm/szae072.

Boutros, S.W., et al., 2021. Effects of alpha-Synuclein targeted antisense oligonucleotides on Lewy body-like pathology and behavioral disturbances induced by injections of pre-formed fibrils in the mouse motor cortex. J. Parkinsons Dis. 11, 1091–1115. https://doi.org/10.3233/JPD-212566.

Brenneman, M., et al., 2010. Autologous bone marrow mononuclear cells enhance recovery after acute ischemic stroke in young and middle-aged rats. J. Cereb. Blood Flow Metab. 30, 140–149. https://doi.org/10.1038/jcbfm.2009.198.

Cai, W., et al., 2019. STAT6/Arg1 promotes microglia/macrophage efferocytosis and inflammation resolution in stroke mice. JCI Insight. https://doi.org/10.1172/jci.insight.131355 e131355.

Chen, D., et al., 2022. Interleukin 13 promotes long-term recovery after ischemic stroke by inhibiting the activation of STAT3. J. Neuroinflammation 19, 112. https://doi.org/10.1186/s12974-022-02471-5.

Coll, R.C., et al., 2015. A small-molecule inhibitor of the NLRP3 inflammasome for the treatment of inflammatory diseases. Nat. Med. 21, 248–255. https://doi.org/10.1038/nm.3806.

Dabrowska, S., et al., 2019. Human bone marrow mesenchymal stem cell-derived extracellular vesicles attenuate neuroinflammation evoked by focal brain injury in rats. J. Neuroinflammation 16, 216. https://doi.org/10.1186/s12974-019-1602-5.

Davis, C., et al., 2021. Mesenchymal stem cell derived extracellular vesicles for repairing the neurovascular unit after ischemic stroke. Cells 10, 767. https://doi.org/10.3390/cells10040767.

Detante, O., et al., 2018. Cell therapy in stroke-cautious steps towards a clinical treatment. Transl. Stroke Res. 9, 321–332. https://doi.org/10.1007/s12975-017-0587-6.

Dhuria, S.V., et al., 2010. Intranasal delivery to the central nervous system: mechanisms and experimental considerations. J. Pharm. Sci. 99, 1654–1673. https://doi.org/10.1002/jps.21924.

Ding, R., Zhang, H., 2021. Efficacy of very early mobilization in patients with acute stroke: a systematic review and meta-analysis. Ann. Palliat. Med. 10, 11776–11784. https://doi.org/10.21037/apm-21-2997.

Doorn, J., et al., 2012. Therapeutic applications of mesenchymal stromal cells: paracrine effects and potential improvements. Tissue Eng. Part B Rev. 18, 101–115. https://doi.org/10.1089/ten.TEB.2011.0488.

Drath, I., et al., 2025. Nose-to-brain drug delivery: from bench to bedside. Transl. Neurodegener. 14, 23. https://doi.org/10.1186/s40035-025-00481-w.

Fu, Y., et al., 2017. Trophic effects of mesenchymal stem cells in tissue regeneration. Tissue Eng. Part B Rev. 23, 515–528. https://doi.org/10.1089/ten.TEB.2016.0365.

Gadani, S.P., et al., 2012. IL-4 in the brain: a cytokine to remember. J. Immunol. 189, 4213–4219. https://doi.org/10.4049/jimmunol.1202246.

Gomez-Galvez, Y., et al., 2024. Recovery after human bone marrow mesenchymal stem cells (hBM-MSCs)-derived extracellular vesicles (EVs) treatment in post-MCAO rats requires repeated handling. PLoS One 19, e0312298. https://doi.org/10.1371/journal.pone.0312298.

Hermann, D.M., et al., 2019. Animal models of ischemic stroke and their impact on drug discovery. Expert Opin. Drug Discov. 14, 315–326. https://doi.org/10.1080/17460441.2019.1573984.

Hu, H., et al., 2022. Exosomes derived from bone marrow mesenchymal stem cells promote angiogenesis in ischemic stroke mice via upregulation of MiR-21-5p. Biomolecules 12, 883. https://doi.org/10.3390/biom12070883.

Ishizaka, S., et al., 2013. Intra-arterial cell transplantation provides timing-dependent cell distribution and functional recovery after stroke. Stroke 44, 720–726. https://doi.org/10.1161/STROKEAHA.112.677328.

Kossmann, T., et al., 1997. Interleukin-8 released into the cerebrospinal fluid after brain injury is associated with blood-brain barrier dysfunction and nerve growth factor production. J. Cereb. Blood Flow Metab. 17, 280–289. https://doi.org/10.1097/00004647-199703000-00005.

Kumari, S., et al., 2024. The impact of cytokines in neuroinflammation-mediated stroke. Cytokine Growth Factor Rev. 78, 105–119. https://doi.org/10.1016/j.cytogfr.2024.06.002.

Lai, S., et al., 2015. Quantitative kinematic characterization of reaching impairments in mice after a stroke. Neurorehabil. Neural Repair 29, 382–392. https://doi.org/10.1177/1545968314545174.

Li, Y., Zhang, J., 2021. Animal models of stroke. Animal Model Exp. Med. 4, 204–219. https://doi.org/10.1002/ame2.12179.

Li, W., et al., 2021. Mesenchymal stem cell-based therapy for stroke: current understanding and challenges. Front. Cell. Neurosci. 15, 628940. https://doi.org/10.3389/fncel.2021.628940.

Liddelow, S.A., 2017. Neurotoxic reactive astrocytes are induced by activated microglia. Nature 541, 481–487. https://doi.org/10.1038/nature21029.

Liu, W., Tang, Y., Feng, J., 2011. Cross talk between activation of microglia and astrocytes in pathological conditions in the central nervous system. Life Sci. 89, 141–146. https://doi.org/10.1016/j.lfs.2011.05.011.

Longo, V., et al., 2022. Transcranial direct current stimulation enhances neuroplasticity and accelerates motor recovery in a stroke mouse model. Stroke 53, 1746–1758. https://doi.org/10.1161/STROKEAHA.121.034200.

Mizrachi, M., Diamond, B., 2024. Impact of microglia isolation and culture methodology on transcriptional profile and function. J. Neuroinflammation 21, 87. https://doi.org/10.1186/s12974-024-03076-w.

Moon, G.J., et al., 2019. Application of mesenchymal stem cell-derived extracellular vesicles for stroke: biodistribution and MicroRNA study. Transl. Stroke Res. 10, 509–521. https://doi.org/10.1007/s12975-018-0668-1.

Morrison, H.W., Filosa, J.A., 2013. A quantitative spatiotemporal analysis of microglia morphology during ischemic stroke and reperfusion. J. Neuroinflammation 10, 4. https://doi.org/10.1186/1742-2094-10-4.

Moulton, C., et al., 2024. Navigating the nano-bio immune interface: advancements and challenges in CNS nanotherapeutics. Front. Immunol. 15, 1447567. https://doi.org/10.3389/fimmu.2024.1447567.

Murphy, S.J., Werring, D.J., 2020. Stroke: causes and clinical features. Medicine (Abingdon) 48, 561–566. https://doi.org/10.1016/j.mpmed.2020.06.002.

Myers, M.I., et al., 2023. Intracerebral transplantation of autologous mesenchymal stem cells improves functional recovery in a rat model of chronic ischemic stroke. Transl. Stroke Res. https://doi.org/10.1007/s12975-023-01208-7.

Natale, F., et al., 2022. Neural stem cell-derived extracellular vesicles counteract insulin resistance-induced senescence of neurogenic niche. Stem Cells 40, 318–331. https://doi.org/10.1093/stmcls/sxab026.

Nedergaard, M., Dirnagl, U., 2005. Role of glial cells in cerebral ischemia. Glia 50, 281–286. https://doi.org/10.1002/glia.20205.

Piepke, M., et al., 2021. Interleukin-10 improves stroke outcome by controlling the detrimental interleukin-17A response. J. Neuroinflammation 18, 265. https://doi.org/10.1186/s12974-021-02316-7.

Podda, M.V., et al., 2014. Extremely low-frequency electromagnetic fields enhance the survival of newborn neurons in the mouse hippocampus. Eur. J. Neurosci. 39, 893–903. https://doi.org/10.1111/ejn.12465.

Sánchez, S.V., et al., 2025. Intranasal delivery of extracellular vesicles: a promising new approach for treating neurological and respiratory disorders. J. Control. Release 379, 489–523. https://doi.org/10.1016/j.jconrel.2025.01.018. Erratum in: J. Control. Release 2025. 383, 113800. Doi: 10.1016/j.jconrel.2025.113800. (PMID: 39800240).

Sanchez-Bezanilla, S., et al., 2021. More than motor impairment: a spatiotemporal analysis of cognitive impairment and associated neuropathological changes following cortical photothrombotic stroke. J. Cereb. Blood Flow Metab. 41, 2439–2455. https://doi.org/10.1177/0271678X211005877.

Saura, J., et al., 2003. High-yield isolation of murine microglia by mild trypsinization. Glia 44, 183–189. https://doi.org/10.1002/glia.10274.

Saver, J.L., et al., 1999. Infarct volume as a surrogate or auxiliary outcome measure in ischemic stroke clinical trials. The RANTTAS Investigators. Stroke 30, 293–298. https://doi.org/10.1161/01.str.30.2.293.

Savitz, S.I., et al., 2011. Intravenous autologous bone marrow mononuclear cells for ischemic stroke. Ann. Neurol. 70, 59–69. https://doi.org/10.1002/ana.22458.

Schallert, T., et al., 2000. CNS plasticity and assessment of forelimb sensorimotor outcome in unilateral rat models of stroke, cortical ablation, parkinsonism and spinal cord injury. Neuropharmacology 39, 777–787. https://doi.org/10.1016/s0028-3908(00)00005-8.

Spinelli, M., et al., 2020. Neural stem cell-derived exosomes revert HFD-dependent memory impairment via CREB-BDNF Signalling. Int. J. Mol. Sci. 21, 8994. https://doi.org/10.3390/ijms21238994.

Steinberg, G.K., et al., 2018. Two-year safety and clinical outcomes in chronic ischemic stroke patients after implantation of modified bone marrow-derived mesenchymal stem cells (SB623): a phase 1/2a study. J. Neurosurg. 131, 1462–1472. https://doi.org/10.3171/2018.5.JNS173147.

Tennant, K.A., et al., 2010. The vermicelli and capellini handling tests: simple quantitative measures of dexterous forepaw function in rats and mice. J. Vis. Exp. 41, 2076. https://doi.org/10.3791/2076.

Tremblay, M.È., et al., 2012. Effects of aging and sensory loss on glial cells in mouse visual and auditory cortices. Glia 60, 541–558. https://doi.org/10.1002/glia.22287.

Tsiapalis, D., O'Driscoll, L., 2020. Mesenchymal stem cell derived extracellular vesicles for tissue engineering and regenerative medicine applications. Cells 9, 991. https://doi.org/10.3390/cells9040991.

Wang, L., et al., 2022. NLRP3 Inflammasome activation: a therapeutic target for cerebral ischemia-reperfusion injury. Front. Mol. Neurosci. 15, 847440. https://doi.org/10.3389/fnmol.2022.847440.

Whishaw, I.Q., et al., 2017. The syntactic organization of pasta-eating and the structure of reach movements in the head-fixed mouse. Sci. Rep. 7, 10987. https://doi.org/10.1038/s41598-017-10796-y.

Xu, W., et al., 2025. NLRP3 inflammasome in neuroinflammation and central nervous system diseases. Cell. Mol. Immunol. 22, 341–355. https://doi.org/10.1038/s41423-025-01275-w.

Yoo, S.W., et al., 2013. Immune following suppression mesenchymal stem cell transplantation in the ischemic brain is mediated by TGF-β. Neurobiol. Dis. 58, 249–257. https://doi.org/10.1016/j.nbd.2013.06.001.

Zbesko, J.C., et al., 2018. Glial scars are permeable to the neurotoxic environment of chronic stroke infarcts. Neurobiol. Dis. 112, 63–78. https://doi.org/10.1016/j.nbd.2018.01.007.

Zhang, Y., et al., 2025. Interleukin-2 and its receptors: implications and therapeutic prospects in immune-mediated disorders of central nervous system. Pharmacol. Res. 213, 107658. https://doi.org/10.1016/j.phrs.2025.107658.

Zhao, et al., 2019. Substrain- and sex-dependent differences in stroke vulnerability in C57BL/6 mice. J. Cereb. Blood Flow Metab. 39, 426–438. https://doi.org/10.1177/0271678X17746174.

Zhou, X., et al., 2023. Intranasal delivery of BDNF-loaded small extracellular vesicles for cerebral ischemia therapy. J. Control. Release 357, 1–19. https://doi.org/10.1016/j.jconrel.2023.03.033.